GEOMECHANICAL EFFECTS ON CO_2 LEAKAGE THROUGH FAULT ZONES DURING LARGE-SCALE UNDERGROUND INJECTION

Antonio P. Rinaldi[(a,*)], Jonny Rutqvist[(a)], Frédéric Cappa[(a,b)]

(a) Lawrence Berkeley National Laboratory, Earth Sciences Division, CA, USA

e-mail: aprinaldi@lbl.gov, jrutqvist@lbl.gov

(b) GeoAzur, University of Nice Sophia-Antipolis, Côte d'Azur Observatory, France

e-mail: cappa@geoazur.unice.fr

(*) Corresponding author at: Lawrence Berkeley National Laboratory, Earth Sciences Division, 1 Cyclotron Road, Berkeley, CA, USA

ABSTRACT

The importance of geomechanics—including the potential for faults to reactivate during large-scale geologic carbon sequestration operations—has recently become more widely recognized. However, notwithstanding the potential for triggering notable (felt) seismic events, the potential for buoyancy-driven CO_2 to reach potable groundwater and the ground surface is actually more important from public safety and storage-efficiency perspectives. In this context, this work extends the previous studies on the geomechanical modeling of fault responses during underground carbon dioxide injection, focusing on the short-term integrity of the sealing caprock, and hence on the potential for leakage of either brine or CO_2 to reach the shallow groundwater aquifers during active injection. We consider stress/strain-dependent permeability and study the leakage through the fault zone as its permeability changes during a reactivation, also causing seismicity. We analyze several scenarios related to the volume of CO_2 injected (and hence as a function of the overpressure), involving both minor and major faults, and analyze the profile risks of leakage for different stress/strain-permeability coupling functions. We conclude that whereas it is very difficult to predict how much fault permeability could change upon reactivation, this process can have a significant impact on the leakage rate. Moreover, our analysis shows that induced seismicity associated with fault reactivation may not necessarily open up a new flow path for leakage. Results show a poor correlation between magnitude and amount of fluid leakage, meaning that a single event is generally not enough to substantially change the permeability along the entire fault length. Consequently, even if some changes in permeability occur, this does not mean that the CO_2 will migrate up along the entire fault, breaking through the caprock to enter the overlying aquifer.

INTRODUCTION

Public concerns always arise when dealing with exploitation of underground natural resources. Ground deformation, induced seismicity, and the potential for groundwater contamination are general issues for public acceptance of projects involving underground fluid injection—e.g., disposal of wastewater or carbon dioxide (CO_2). The potential for injection-induced fault reactivation associated with industrial injection activities is an important issue, not just from a safety point of view, but also from a public acceptance perspective (Kerr, 2012). The correlation between underground fluid injection and seismicity is an issue that has been extensively studied (e.g., Shapiro and Dinske, 2009; Garagash and Germanovich, 2012; National Research Council, 2012). Fluid movements may control the fault activity in the continental crust (e.g., Leclère et al., 2012), and fluid-rock interaction may be associated with so-called fault-valve behavior over geological time (Sibson, 1990). A recent review work by Manga et al. (2012) highlights how transient stress in the crust may affect the permeability along fault zones. This review paper shows the relationship between the observed seismicity and the water level in wells close to the earthquake epicenter. With respect to natural seismicity, it is hard to discriminate between the relative contributions of induced fluid pressure and tectonic stress, but there are plenty of examples in the literature relating fluid overpressure to local seismic events. One such well-known case is hydraulic stimulation associated with an enhanced geothermal field development in Basel, Switzerland, where an earthquake of magnitude 3.4 occurred (e.g., Bachmann et al., 2011; Terakawa et al., 2012). Another example is disposal of water into the Ozark Aquifer of Arkansas, where a few earthquakes of magnitude greater than 4 were felt by the local population (Kerr, 2012).

Although carbon capture and storage (CCS) has been recognized as a promising option for reducing CO_2 emissions into the atmosphere (Pacala and Socolow, 2004), there are concerns related to the potential for triggering notable (felt) seismic events, and how such events could impact the long-term integrity of a CO_2 repository (as well as how it could impact the public perception of geological carbon sequestration) (Zoback and Gorelick, 2012). To date, no felt seismic event induced by CCS has occurred. Geomechanical processes and issues associated with geological carbon sequestration have recently received more attention. A state-of-the-art review can be found in Rutqvist (2012), which describes the various possible effects resulting from CO_2 injection into a deep sedimentary basin, including reservoir stress-strain and microseismicity (e.g., Zhou et al., 2010; Myer and Daley, 2011), caprock sealing performance (e.g., Vilarrasa et al., 2010; Hou et al., 2012), and the potential for fault reactivation (e.g., Cappa and Rutqvist, 2011a; Nicol et al., 2011). Moreover, several studies have recently shown how CO_2 injection may produce seismic events both on major faults (i.e., large faults with large initial shear offset—Cappa and Rutqvist, 2011a,b,2012), and on minor faults that might have gone undetected during the site characterization, e.g., faults less than 1 km long and without detected initial offset (Mazzoldi et al., 2012). Although the potential for triggering felt seismic events is one major issue that may play a role in public acceptance of geological carbon sequestration, it is very important from safety and storage-efficiency perspectives to evaluate the potential for buoyancy-driven CO_2 to reach potable groundwater and the ground surface. Several studies have also shown that the overpressure needed to inject carbon dioxide into a deep saline formation may displace the brine vertically (e.g., Birkholzer et al., 2011; Oldenburg and Rinaldi, 2011) or horizontally (e.g., Nicot, 2008). Moreover, recent analyses have been focused on leakage pathways at specific sites, such as at the Cranfield, MS, USA (e.g. Nicot et al., 2013), or at In Salah, Algeria (e.g. Shi et al., 2012; Rinaldi and Rutqvist, 2013), and other studies have also

considered the impact of caprock hydraulic parameters on potential leakage (Hou et al., 2012). However, one important question that needs to be addressed is: How could fault reactivation affect the sealing properties of a storage site? Could permeability be substantially increased along with fault reactivation, and could such reactivation open up a new preferential pathway along which for fluids to leak?

Typically, geological observations describe the structure of fault zones as single or multiple narrow core zones (often less than 10 cm, and, in many cases, less than 1 cm in thickness) surrounded by an intensively fractured damage zone, the width of which can range from 1 m to several hundreds meters (Fig. 1) (Vermilye and Scholz, 1998; Ben-Zion and Sammis, 2003; Sibson, 2003; Wilson et al., 2003; Wibberley and Shimamoto, 2003; Faulkner et al., 2006; Mitchell and Faulkner, 2009). Core zones correspond to localized slip zones containing highly deformed gouge, breccias, cataclasites, and ultracataclasites. The damage zone is generally composed of fractured rock, which is in turn surrounded by less fractured host rock. Strong contrasts in properties (typically seismic velocity, permeability, and rigidity) have been measured for each component of fault structure and the surrounding host rock (Faulkner and Rutter, 1998; Wibberley and Shimamoto, 2003; Gudmundsson, 2004; Faulkner et al., 2006; Cappa et al., 2007; Guglielmi et al., 2008; Gudmundsson et al., 2010; Jeanne et al., 2012a,b,2013a). These observations have revealed that the permeability and Young's modulus of a fault zone may vary significantly (several orders of magnitude) with distance from the principal slip zone itself—that is, from the core through the fractured damage zone and to the less fractured host rock. These fractures generally make the damage zone more permeable than the core, and the gouge makes the core less rigid than the damage zone. Permeability within the fault core (~1×10^{-17} to 1×10^{-21} m^2) can be several orders of magnitude smaller than that in the

damage zone (~1×10^{-14} to 1×10^{-16} m^2) (Faulkner and Rutter, 1998; Wibberley and Shimamoto, 2003). Moreover, while the fault core may actually prevent the flux through the fault zone, upward CO_2 may still migrate along the more permeable damage zone. Similarly, the Young's modulus is generally lower in the fault core (~1 to 10 GPa) than in the damage zone (~10 to 70 GPa) (Faulkner and Rutter, 1998; Gudmundsson, 2004).

Crustal-scale permeability-depth relations can be estimated using geothermal data and the fluid flux during prograde metamorphism. Manning and Ingebritsen (1999) found this relation to be $\log \kappa \sim -14 - 3.2 \log z$. However, there are several evidences that the permeability may reach much higher values (over short time scales) when considering seismically active regions, especially during a strong aftershock sequence as induced by pressure propagation in the rock surrounding the fault region (Noir et al., 1997; Miller et al., 2004). Recently, Ingebritsen and Manning (2010) compared data from tectonically active regions, and found a permeability-depth relationship of $\log \kappa \sim -11 - 3.2 \log z$ — similar to what they found in their previous work, but with higher permeability values for the same depth. In this paper, we aim to study a region that is not seismically active, and that is only reactivated after the CO_2 injection. The initial permeability is then in line with the equation suggested by Manning and Ingebritsen (1999) for a nonseismically active region (i.e. $\log k \sim -14 - 3.2 \log z$), and this permeability should represent an average value at injection depth that can be locally lower at fault core (e.g. Faulkner and Rutter, 1998)

This work extends previous geomechanical modeling using the TOUGH-FLAC simulator (Rutqvist et al., 2002; Rutqvist, 2011). The TOUGH-FLAC simulator has been applied and tested over a wide range of geoscientific fields and geoengineering applications, including

enhanced geothermal systems (Rutqvist et al., 2013a; Rinaldi et al., 2013), hydrothermal systems and volcanology (Todesco et al., 2004), fault reactivation and hydraulic fracturing during shale gas operations (Rutqvist et al., 2013b), gas production from hydrate-bearing sediments (Rutqvist et al., 2012b), nuclear waste disposal (Rutqvist and Tsang, 2012, and references therein), compressed air enhanced systems (e.g., Rutqvist et al., 2012a), as well as carbon sequestration (e.g., Rutqvist and Tsang, 2002; Cappa and Rutqvist, 2012; Rinaldi and Rutqvist, 2013). Following Cappa and Rutqvist (2011b) and Mazzoldi et al. (2012), the approach for modeling fault reactivation adopted here involves coupled fluid flow, as well as geomechanical numerical modeling and theories from seismology, to calculate seismic source parameters. A strain-softening fault constitutive model enabled us to model sudden co-seismic fault rupture and hence to evaluate the seismic magnitude.

This work aims to study the fault responses during underground CO_2 injection, focusing on the short-term (5 years) integrity of the CO_2 repository, and hence on the potential leakage of CO_2 to shallow groundwater aquifers. Increased pore pressure can alter the stress distribution on a fault/fracture zone, which may produce changes in the permeability related to the elastic and/or plastic strain (or stress) during single (or multiple) shear ruptures. We account for stress/strain-dependent permeability and study the leakage through the fault zone as its permeability changes along with strain and stress variations. We analyze several scenarios related to the injected amount of CO_2 (and hence related to potential overpressure) involving both minor and major faults, and analyze the risk of leakage for different stress/strain-permeability coupling functions.

MODELING SETUP

In this section, we introduce the modeling approach that we used to estimate the effects of different CO_2 injection rates on upper aquifer leakage, and the potential for fault reactivation for two different scenarios.

Scenario #1 is basically the one presented in Mazzoldi et al. (2012), with a minor, 1 km long fault zone intersecting a 100 m thick injection aquifer bounded by a 150 m thick low-permeability caprock (Fig. 2a). This scenario aims to represent a fault that is difficult to detect by seismic survey, since it would have shear offset of less than 10 m.

Scenario #2, first presented in Cappa and Rutqvist (2011a,b), represents a fault zone having a large shear offset (on the order of hundreds of meters), meaning that it would also be very large. Also in this case, the fault zone intersects a 100 m thick reservoir confined on the upper and bottom parts by a 150 m thick caprock. However, with this scenario, we want to simulate a major, easy-to-detect fault zone, with an offset of 100 m (Fig. 2b). This scenario was also recently used for simulating the dynamic behavior of fault reactivation during underground CO_2 injection (Cappa and Rutqvist, 2012).

The two scenarios were chosen to represents close-to-worst-case conditions, i.e. a subvertical fault in a stress regime (normal faulting) that is near critically stressed for fault reactivation, with (in this case) a lower horizontal stress. Such conditions have the effect of reactivating the fault zone with only a few MPa increase in pressure, if an initial shear offset along the fault is assumed. For a subhorizontal fault, the reactivation would never result in a slip upward through the caprock, and hence no leakage would be observed. Scenario #1 is based on the likelihood

that, if the volume of injection were very large (as it would probably be at a future industrial-scale CO_2 sequestration site), a minor fault with this configuration would be encountered.

We analyzed the short-term fault response during active CO_2 injection in terms of displacement and as a pathway for leakage, and then we applied empirical moment-magnitude relations (e.g., Kanamori and Anderson, 1975) to estimate the corresponding seismic magnitude. We simulated different rates of CO_2 injection for both scenarios. Moreover, since changes in permeability and porosity may occur, we simulated three different cases of coupling between mechanical and hydraulic properties.

Mechanical effects on porosity and permeability

The hydraulic properties of a deformable porous and fractured medium, such as faults, may change as pressure and stresses evolve (Rutqvist and Stephansson, 2003). Depending on the fault (and fracture reactivation), changes in hydromechanical properties may be isotropic or anisotropic. Isotropic changes can be assumed in a nonfractured fault core, or in the damage zone when highly fractured, where the anisotropy is small and fractures might be assumed to be randomly distributed. In such cases, permeability and porosity changes may be simply related to changes in volumetric strain or mean stress. We will evaluate the effects of changes in permeability and porosity on fault reactivation and CO_2 leakage after a few years of injection, accounting for two different isotropic models. The first model (Case1) relates the porosity (ϕ_{hm}) to the mean effective stress (σ'_M), with permeability (κ_{hm}) depending on the porosity changes. The formulation was first derived based on laboratory data by Davies and Davies (2001), and

then modified for stress-dependent permeability in reservoir rocks and fracture zones by Rutqvist and Tsang (2002):

$$\begin{cases} \phi_{hm} = (\phi_0 - \phi_r)\exp(5 \cdot 10^{-8} \cdot \sigma'_M) + \phi_r \\ \kappa_{hm} = \kappa_0 \exp[22.2(\phi_{hm}/\phi_0 - 1)] \end{cases} \quad (1)$$

where subindex *0* refers to the initial unstressed value (for both porosity and permeability, ϕ_0 and κ_0), and ϕ_r is the residual porosity at high stress. We applied the changes to the fault zone only, with a residual porosity of 5%. Rutqvist and Tsang (2002) also applied Eq. 1 with a 5% residual porosity for a fault, representing permeability changes in highly fractured rock along the fault. The mean-stress approach is valid for randomly oriented fracture networks, as would be the case if most permeability changes occur in the damage zone. Indeed, the original function was fitted to sandstone, but it was for a very small porosity change range, from 0.09 to 0.1. For fractured rock, we have chosen the initial porosity (ϕ_0) and residual porosity (ϕ_r) such that we can get a several orders-of-magnitude change — from residual fracture porosity (ϕ_r) to completely jacked open fractures under fluid pressurization (ϕ_0). Then, the actual permeability changes during the simulation depend on the actual changes in mean stress, in this case up to 2-to-3 orders of magnitude.

The second case (Case2) relates porosity to the isotropic volumetric strain variation, and again, permeability is then related to changes in porosity. This model was developed and applied by Chin et al. (2001) for modeling of permeability changes in a petroleum reservoir, and then modified by Cappa and Rutqvist (2011b) to account for permeability changes in a fault zone after reactivation because of underground CO_2 injection:

$$\begin{cases} \phi_{hm} = 1 - (1 - \phi_0)\exp(-\varepsilon_V) \\ \kappa_{hm} = \kappa_0(\phi_{hm}/\phi_0)^{15} \end{cases} \quad (2)$$

where ϕ_{hm} and κ_{hm} are the porosity and the permeability at a given stress, ϕ_0 and κ_0 are the initial porosity and permeability, respectively, and ε_V is the total volumetric strain (both plastic and elastic). The empirical permeability-porosity function in Eq. 2 has been shown to be widely applicable to geological materials. Even if the exponent could vary between 3 and 25 for consolidated geological materials (David et al., 1994), we set the exponent to 15, following Cappa et al. (2011b), for a 2-to-3 order-of-magnitude increase upon reactivation. With respect to the previous formulation (Eq. 1), the relation between porosity and the total volumetric strain in Eq. 2 accounts for both elastic and plastic behavior that may occur during fault reactivation.

In a fractured fault core, changes in permeability and porosity may be extremely anisotropic, depending on fracture direction. Then, the hydraulic parameters depend on anisotropic elasto-plastic properties: the permeability may depend on both the fault normal stress and on the plastic shear and tensile strain. Hsiung et al. (2005) derived the relation between these parameters and both the porosity and permeability of a fractured media with one set of uniformly spaced fractures. Here, we apply the same formulation for a fault zone (Case3). Following their approach, we can assume change in porosity caused by plastic deformation:

$$\begin{cases} \phi_{hm} = \phi_0 + \Delta\phi_{fp} \\ \Delta\phi_{fp} = e_{ftp} + e_{fsp}\tan\psi \end{cases} \quad (3)$$

where $\Delta\phi_{fp}$ are the changes in porosity. e_{ftp} and e_{fsp} are the plastic strains caused by tensile and shear deformation, respectively, and ψ represents the fault dilation. The permeability changes are then based on a nonlinear function of the effective normal stress (σ'_n), as well as on the plastic strain:

$$\begin{cases} \kappa_{hm} = \kappa_0 \left[\frac{a}{c(c\sigma'_n+1)} \sqrt{\frac{\phi_0}{12\kappa_0}} + \frac{e_{ftp}+e_{fsp}\tan\psi}{\phi_0} \right] \\ a = K^{-1} \\ c = \frac{-1\pm\sqrt{1+4\sigma'_{n0}a\sqrt{\phi_0/\kappa_0}}}{2\sigma'_{n0}} \end{cases} \quad (4)$$

a and c are two empirical constants for the normal-closure hyperbola (Bandis et al., 1983) that in Eq. 4 are related to the initial normal stiffness (K), initial effective normal stress (σ'_{n0}), initial porosity (ϕ_0), and initial permeability (κ_0). A complete description of the constants a and c, and their derivation, can be found in Hsiung et al. (2005).

In addition to the coupling equations for porosity and permeability, for each case the capillarity pressure (p_c) varies according to a function by Leverett (1941):

$$p_c = p_{c0}(S_l)\sqrt{\frac{\kappa_0/\phi_0}{\kappa_{hm}/\phi_{hm}}} \quad (5)$$

where $p_{c0}(S_l)$ is the unchanged capillarity pressure, which depends on the liquid saturation (S_l). This equation for the capillarity pressure is applied for each of the three cases analyzed.

Seismic event modeling and magnitude estimation

The injection of CO_2 in the storage aquifer will produce an increase in pore pressure. The normal stress acting across a fault zone is already reduced to the effective value because of native water, according to Terzaghi (1923):

$$\sigma_n' = \sigma_n - p \quad (6)$$

where σ'_n is the effective normal stress, σ_n is the total stress, and p is the pore pressure. An increase in pore pressure due to CO_2 injection will furthermore reduce the effective normal stress (σ'_n). Following previous studies, the fault zone is simulated using a ubiquitous-joint fractured medium (e.g. Cappa and Rutqvist, 2011a), representing strongly anisotropic strength behavior, represented by the orientation of weakness (fault plane) in an elasto-plastic Mohr-Coulomb constitutive model. In a fault with a given orientation, the Mohr-Coulomb criterion for failure can be written as (Jaeger and Cook, 1979):

$$\tau = c + \mu_s \sigma_n' \quad (7)$$

where τ is the critical shear stress (i.e., shear strength) necessary for slip occurrence, c is the cohesion, and μ_s is the static friction ($\mu_s = \tan \varphi$, where φ is the friction angle). For most rocks, the static friction ranges between 0.6 and 0.85 (Cappa and Rutqvist, 2011b, and references therein). To enable the capturing of a sudden slip (i.e., seismic event), we used a Mohr-Coulomb model with strain-softening frictional strength properties, consistent with a seismological slip-weakening fault model. In our quasi-static model, the frictional coefficient varies from a static

value of 0.6 to a value of 0.2 when the strain on the fault zone is greater than a certain critical value (10^{-3}), and a rupture occurs (Cappa and Rutqvist, 2011a,b).

In a two-dimensional plane, the normal and shear stress acting on the fault plane (a line in a 2D model, Fig. 2) can be written as:

$$\begin{cases} \sigma_n = \frac{1}{2}(\sigma_v + \sigma_h) - \frac{1}{2}(\sigma_v - \sigma_h)\cos 2\delta \\ \tau = \frac{1}{2}(\sigma_v - \sigma_h)\sin 2\delta \end{cases} \quad (8)$$

where σ_v is the vertical stress (in this case the maximum principal stress), σ_h is the minimum horizontal stress (in this case also the minimum principal stress), and δ is the angle between the fault plane and the maximum principal stress direction (in this case 10˚). According to Eq. 7, slip (shear failure) will be induced as soon as the shear stress (τ) equals the shear strength (τ_s), and for a cohesionless fault (c = 0), the slip will occur once the so-called ambient stress ratio (τ/σ'_n) exceeds the coefficient of static friction (μ_s).

These equations can be still applied to a three-dimensional case in which a fault strikes parallel to the intermediate principal stress, which in this example would be the maximum horizontal stress (σ_H); the subsequent generalization to a full three-dimensional formulation is not difficult (Beer and Johnson, 1992).

Following the approach used by Cappa and Rutqvist (2011a,b; 2012) and Mazzoldi et al. (2012), the magnitude of a seismic event is estimated using empirical moment-magnitude relations. The

seismic moment (M_0) is first estimated for a ruptured patch on a fault following the well-known equation (e.g. Kanamori and Brodsky, 2004)

$$M_0 = GAd \quad (9)$$

where G is the rigidity (or shear modulus) of the medium (Pa), A is the rupture area (m^2), and d (m) is the average slip resulting along the fault zone when the shear stress drops and the frictional coefficient changes (Cappa and Rutqvist, 2011a,b,2012; Mazzoldi et al., 2012). In our 2D model, the rupture area (A) is considered to be circular, with a diameter equal to the rupture length simulated along the fault line, i.e., the rupture area is considered to be normal to the 2D plane and aligned with the intermediate stress.

The seismic magnitude can then be estimated by the equation proposed by Kanamori and Anderson (1975):

$$M = (\log_{10} M_0/1.5) - 6.1 \quad (10)$$

where the seismic moment (M_0) is in N·m. In our modeling, we are able to distinguish between the co-seismic fault slip (d), which is used to give an estimate of the seismic event, and the aseismic slip, which may produce a larger shear displacement on the fault plane, but is not causing seismicity.

Numerical model and conditions

Numerical simulations were carried out using the coupled fluid flow and geomechanical simulator TOUGH-FLAC (Rutqvist, 2011) based on the multiphase, multicomponent fluid flow and heat transport simulator TOUGH2 (Pruess et al., 2011) and on the geomechanical simulator FLAC^{3D} (ITASCA, 2009). TOUGH-FLAC has been applied to several problems relating deformation and fluid flow during underground CO_2 sequestration (e.g., Rutqvist and Tsang, 2002; Rutqvist et al., 2010,2011; Cappa and Rutqvist, 2011a,b,2012; Mazzoldi et al., 2012; Rinaldi and Rutqvist, 2013). We used the ECO2N module, for which the equation of state for mixtures of water, NaCl, and CO_2 was developed as applied to carbon sequestration studies (Pruess, 2005). The module reproduces, within the experimental error, the thermodynamics and thermophysical properties for the temperature, pressure and salinity conditions of interest (10 ˚C $\leq T \leq$ 110 ˚C; $P \leq 600$ bar; salinity up to full halite saturation). Simulations can be run either isothermally or nonisothermally, while phase conditions can be represented as a single (aqueous or CO_2-rich) phase or two-phase mixture. The fluid phase may appear or disappear, and the solid salt may precipitate or dissolve.

In both of the scenarios considered in this work (Fig. 2), the fault zone consists of a fault core bounded by a damage zone, which corresponds to a more permeable zone with a macroscopic fracture network (Fig. 1b; Cappa and Rutqvist, 2011a, and references therein). For the aims of this work, we simulated the fault core using a ubiquitous joint model, with finite thickness elements having anisotropic elasto-plastic properties (Table 1) and intensely jointed along a direction parallel to the fault plane—thus permitting the shear failure to occur along the fault itself. The damage zone is simulated as a poro-elastic medium (no slip occurs within the damage

zone) with finite thickness elements that have the same high permeability as the fault core and that can be subject to permeability changes due to variation in stress and/or strain. Such a fault zone (damage zone plus fault core) intersects a 2D plane-strain multilayer system (2 km × 2 km) with a dip angle of 80˚ and a length of 1 or 2 km (according the selected scenario, Fig. 2). The storage formation is 100 m thick and bounded at the top and bottom by a low-permeability 150 m thick formation, which, in turn, is surrounded by two other aquifers. Hydraulic and mechanical properties for the different layers (aquifers and caprock) are equal for both scenarios and are listed in Table 1 (after Cappa and Rutqvist, 2011a). These properties were kept constant during all the simulations performed, with the exception of the fault-zone properties.

We set the initial conditions assuming specific linear pore pressure and temperature gradients (9.81 MPa/km and 25˚C/km, respectively), with atmospheric pressure of 0.1 MPa and temperature of 10˚C at the ground surface, resulting in a pore pressure of 5 MPa and temperature of 22.5˚C at the top boundary of our model (at 500 m depth). One of the most important parameters related to the reactivation of a fault zone is the initial *in situ* stress (Cappa and Rutqvist, 2011b; Mazzoldi et al., 2012). Mazzoldi et al. (2012), showed, for example, that the maximum earthquake magnitude for an undetected fault (1000 m long) may change from 2.7 to 3.5 when the stress ratio between horizontal (minimum) and vertical (maximum) stress varies within the range of a few percent (from 0.7 to 0.65). For all the simulations in this study, we kept a stress ratio (σ_h/σ_V) of 0.7, which is already a near-critical value for a fault striking along the intermediate horizontal stress, but may prevent (in some cases) the rupture from extending over the entire length of the fault zone (Cappa and Rutqvist, 2011b). Hence, we set the vertical stress gradient to 22,148 Pa/m and the corresponding horizontal stress gradient to 15,504 Pa/m. Using these gradients, the vertical stress and horizontal stresses at the depth of the reservoir (1500 m)

are respectively 33.2 and 23.3 MPa. At a real site, these stress values are important for controlling the injection pressure. For example, the vertical (or lithostatic) stress can easily be estimated from the weight of the overburden rock mass, and the injection pressure would be controlled to be below this value in order to avoid adverse mechanical effects such as fracturing. The horizontal stress might not be known or only estimated with considerable uncertainty, but is an important parameter to consider in order to avoid vertical fracturing of the caprock.

Boundaries were open for fluid flow (i.e., at constant pressure and temperature), except for the left boundary, where no flow occurred. Null displacement conditions were set normal to the left and bottom boundaries, whereas constant stress was imposed normal to the right and top boundaries (Fig. 2). The simulations were conducted in an isothermal mode, implying that the temperature gradient is maintained during the simulation, guaranteeing CO_2 under supercritical conditions at injection. Thermal effects may have an impact on the CO_2 distribution and conditions (e.g., viscosity, density). Temperature variations mostly impact the buoyancy effects; they will only slightly change the current results, which depend mostly on the fault permeability and pressure distribution. In terms of geomechanics, thermal effects may increase or decrease the poro-elastic deformation before fault reactivation, i.e., the time when a seismic event occurs (if it occurs) could be different. Moreover, the injection lasts for 5 years only and cooling would likely occur only in the region close to the injection well, although remarkable effects can arise over 30 years of injection.

We accounted for relative permeabilities and capillarity pressure using the van Genuchten (1980) functions. Van Genuchten parameters are listed in Table 1. CO_2 wettability and viscosity are implicitly considered within TOUGH2. Changes in viscosity increase or decrease the leakage

rate once the entire fault is filled with CO_2. A detailed discussion can be found in Rutqvist et al. (2007).

Two critical parameters in evaluating the short-term leakage and fault reactivation are (1) the initial fault permeability and (2) the CO_2 injection rate. For both scenarios, the initial permeability of the fault zone was varied from 10^{-16} to 10^{-14} m^2. Although sometimes the permeability of the fault core may be much smaller, ranging from 10^{-17} to 10^{-21} m^2, the values we selected are representative of the damage-zone permeability (Gudmundsson, 2000; Faulkner et al., 2006), which mostly affects fluid migration along a fault zone. The fault core and damage zone are discretized into a 3-block-wide zone, but with a small total width; hence, we represent the fault-zone permeability as homogeneous and corresponding to the damage-zone permeability (i.e., permitting the fluid to flow along the fault itself). The Young's modulus of the fault zone was set to 5 GPa (Gudmundsson, 2000; Faulkner et al., 2006).

The second critical parameter is the injection rate. The amount of CO_2 injected may vary from site to site. For example, at the In Salah (Algeria) CO_2 storage project, the injection occurred over three horizontal wells at a rate of about 0.5–1.0 million tons/yr, which corresponds to an average injection rate per well of about 10–15 kg/s (Shi et al., 2012; Rinaldi and Rutqvist, 2013). In our simulations for Scenario #1 (Fig. 2a), CO_2 is injected as a point source at 1500 m depth, with a constant rate ranging from 0.002 to 0.1 kg/s/m, which would correspond, for a horizontal well 1000 m long, to an injection rate ranging from a reasonable low rate of 2 kg/s up to a very high rate of 100 kg/s. Note that the high rate (100 kg/s) is still less than what would be supplied from a typical coal power plant (Rutqvist and Tsang, 2002). Moreover, it is not unrealistic even with a rate 10 times that at In Salah, since the permeability in this example is about 1 order of

magnitude higher than that of In Salah, and the reservoir in this example is 5 times thicker, leading to 50 times higher transmissivity. For Scenario #2 (Fig. 2b), however, we needed to decrease the range from 2 to 12 kg/s, because the fault offset of 100 m results in a hydraulically confined CO_2 reservoir bounded on the right side by the offset part of the caprock. A higher injection rate would result in a rapid pore-pressure increase up to unrealistic values, and since the pressure should be one of the parameters monitored and controlled during injection, such an extreme pressure increase would not be allowed at a real storage project.

We carried out a large number of forward simulations, accounting for seven injection rate values (i.e., logarithmic scale for the Scenario #1 and linear scale for the Scenario #2) and five initial permeability fault values (i.e., every half-order magnitude for both scenarios). In total, 35 simulations were performed for each case of stress/strain-permeability coupling, i.e., about 100 simulations for each scenario.

RESULTS

In this section, the results of the two scenarios (Fig. 2) are analyzed. For each scenario, we first analyzed the amount of CO_2 that could leak into the upper aquifer as a function of the initial fault permeability and injection rate. According to Hepple and Benson (2005), a CO_2 storage project would be considered acceptable from a storage efficiency perspective if the amount of CO_2 leaking into a shallow potable water aquifer or ground surface were less than 0.1% per year. In our study, we focus only on the CO_2 that might leak through the fault zone within a short time of active injection (5 years). Then, at the end of the injection, assuming a maximum leakage rate of 0.1% per year, our threshold would be 0.5% of the total injected CO_2 over the entire 5-year

period. In this study, we define the CO_2 as "leaked" as soon as it migrates up above the single caprock layer, i.e., migrates above a 1300 m depth. This might be a very conservative definition, since at many injection sites, the overburden might consist of multiple layers, and leakage may be related to CO_2 migrating out of a storage complex into much shallower aquifers or the ground surface. Still, with a clear definition and a quantitative threshold values, i.e., 0.5% over 5 years in this case, we are able to compare the different scenarios and determine the critical parameters to be considered in the assessment of the potential for leakage associated with faults and fault reactivation, and this knowledge can be transferred to the analysis of real future CCS sites.

In addition to the analysis of leakage rates, we evaluated the potential for induced seismicity associated with injection-induced fault reactivation and the magnitude of the main seismic event (if any) as a result of a sudden (rapid) slip. Also in this case, the magnitude was analyzed as a function of the initial fault permeability and injection rate. Although the quantitative estimation of the moment magnitudes in our analysis are uncertain considering our simplified 2D model, we can still compare different cases and assess the relative potential for induced seismicity and event magnitudes in each case.

Scenario 1

Resulting leakage percentage for the scenario with a minor, undetected fault (1 km long) for three different cases are shown in Fig. 3. Fig. 3a shows the results for Case1, in which the permeability changes as a function of the mean stress (Eq. 1). The leakage rate is well below the 0.5% threshold, except in the case of a relatively high initial fault permeability, but only if the injection rate is very high. For example, as shown in Fig. 3a, no CO_2 leakage occurs after five years of injection when the initial permeability is relatively low (10^{-16} m^2), even after injecting at the highest rate of 100 kg/s. Fig. 3b shows an example when the injection rate is 20 kg/s, in

which case the initial permeability is relatively low, and permeability changes are limited to less than half an order of magnitude, the CO_2 is confined within the injection reservoir, and no significant upward CO_2 migration occurs. However, if the initial permeability of the fault is as high as 10^{-14} m^2, and if the injection rate is very high (100 kg/s), then about 30% of the injected CO_2 would reach the upper aquifer within 5 years (Fig. 3a). Results show that in this case, the plume quickly moves upward along the fault zone, and after 5 years of injection, the plume reaches the upper aquifer at a depth of about 600 m (Fig. 3c). The permeability increases by one order of magnitude already after the first year of injection, and then rebounds to a half-order-magnitude increase after 5 years. This rebound in permeability is a result of decreasing fluid pressure within the fault, since pressure can be released into the upper reservoir along with leakage of brine and CO_2. It is worth noting that even for very high permeability, the leakage rate would be less than 5% if the injection rate were kept below 10 kg/s, which is still a good injection rate for a CO_2 storage project (Fig. 3a).

Fig. 3d shows the resulting leakage percentage for Case2, in which the permeability changes as a function of the total volumetric strain (Eq. 2). The results show a trend similar to Case1 for high initial fault permeability, with a permeability change of about one order of magnitude and a maximum of 25% leakage when the injection rate is 100 kg/s (Fig. 3f)—whereas no significant leakage occurs when the injection rate is lower than 10 kg/s (Fig. 3d). However, the trend is completely different for permeability lower than 10^{-15} m^2. In fact, while Eq. 2 with a 0.01 volumetric strain may produce up to 5-order-of-magnitude permeability changes within the fault core (where the strain may reach very high values in the worst case), the permeability changes are small in the damage zone, which undergoes only small strain. In this environment, the pressure would increase substantially for a high injection rate. Then, once the fault starts to

reactivate, the reservoir is already substantially overpressurized, and this pressure can only escape through the reactivating fault.

Fig. 3d shows the region where the injection pressure reaches a value greater than 35 MPa: a value barely exceeding the lithostatic (vertical) stress and much greater than the minimum principal stress at the same depth. For these values of pressure, the leakage percentage may reach values up to 40%. Fig. 3e shows the results for the case with a relatively low injection rate (20 kg/s) and low initial fault permeability (10^{-16} m^2), which increases by one order of magnitude already after the first year of injection. After 5 years the permeability is increased by two orders of magnitude in the part of the fault bounded by the upper part of the caprock, where the volumetric strain increases substantially when the fluids are passing through, resulting in a leakage of brine and CO_2 of about 4% of the total injected CO_2.

Finally in Case3, we simulated the permeability and porosity as a function of the normal stress and plastic strain (Eqs. 3 and 4). Results are shown in Fig. 3g: the percentage of leakage in this case is very similar to Case1, but with slightly higher values for very high injection rates (greater than 70 kg/s). A leakage exceeding the 0.5% threshold occurs only for very high injection rates (greater than 30 kg/s). Figures 3h and 3i show two resulting CO_2 plume and permeability changes for a case with 20 kg/s injection rate with initial permeability 10^{-16} m^2 and 100 kg/s injection rate with initial permeability 10^{-14} m^2, respectively. The plumes for these two simulations are very similar to the plumes for corresponding simulations in Case1, although the permeability changes are slightly different, with more changes in Case3, especially within the fault section bounded by the caprock.

In terms of induced seismicity, with our model, it is very likely to trigger a seismic event within this scenario only for high injection rates (Fig. 4). Specifically, Case1 features events of at least magnitude 2 only for injection rates greater than 30 kg/s and initial permeabilities lower than 10^{-15} m^2 (Fig. 4a). With initial low permeability (10^{-16} m^2), the rupture length and mean slip along the fault depend on the injection rate (Fig. 4b). As the permeability increases, the fault reactivation requires a higher injection rate (Fig. 4a and c). For low injection rates, the overpressure never reaches a limit value that would induce an earthquake (red and black lines in Fig. 4c), and when the initial fault permeability is high, the overpressure distributes much faster along the fault, avoiding the pressure buildup within the fault zone (Fig. 4a). In the worst-case scenario, the high overpressure due to high injection rate (100 kg/s) may distribute along the fault, producing a larger rupture at the time of failure (green line in Fig. 4c).

For Case2, some events occur at lower injection rates, since (as explained above) the permeability changes occur mostly within the fault core and not in the damage zone, allowing a greater pressure for lower injection rates, and increasing the probability for triggering seismicity (Fig. 4d). In fact, an event of magnitude 2.7 occurs for an injection rate of 20 kg/s and initial fault permeability of 10^{-16} m^2 (Fig. 4e). A higher initial fault permeability requires a higher injection rate to trigger an event. Fig. 4f shows the resulting displacement for injection rates of 20 kg/s (black line), 50 kg/s (red line), and 100 kg/s (green line) for a fault with initial permeability of 10^{-15} m^2. Note that a bigger displacement occurs for the 50 kg/s injection rate compared to the 100 kg/s case. This is because the event for the lower injection rate occurs at a later time (85 days compared to the 27 days of the 100 kg/s case), thereby allowing the pressure to distribute more extensively along the fault, triggering a larger rupture.

Case3 is also similar to Case1 in terms of seismic magnitude, except that in Case3, seismic events are also likely to occur for a fault permeability up to 10^{-15} m^2 (Fig. 4g). In fact, for low initial fault permeability, the slip occurring on a fault is very similar to Case1 (Fig. 4h), although the rupture area is a little smaller for an injection rate of 50 kg/s (red line). A similar slip to that in Case1 occurred for a higher initial fault permeability and high injection rate (100 kg/s, green line in Figs. 4c and 4i). However, in Case3, seismic events may occur also for lower injection rates, although such events would require a much longer time for the fault to be reactivated (Fig. 4i, red line - 215 d), hence reactivating a larger area, producing a larger event (M = 3.6).

The magnitude of seismic events and the percentage of leakage are not always correlated, and when an event occurs, a high, short-term leakage is not always associated with that kind of scenario. For example, in Case1, a seismic event of magnitude 3 occurs for a permeability of $3 \cdot 10^{-16}$ m^2, but still no leakage is observed after five years of injection at more than 50 kg/s. The poor correlation means that a single event was in this case not enough to substantially change the permeability along the entire fault length. Consequently, even if some changes in permeability occur, this does not mean that the CO_2 would be able to migrate along the entire fault, breaking through the caprock and entering the overlying aquifer.
However, after the first slip, stresses on the fault dissipate along with shear and friction, and our slip-weakening model does not permit the stress to accumulate after the first drop. Therefore, the current analysis does not consider the effects of multiple seismic events.

Fig. 5 shows an example of fluid-pressure temporal evolution at the injection point, with a rate of 100 kg/s for the three cases (green line for Case1, black line for Case2, and red line for Case3) with initial permeability 10^{-16} m^2 (Fig. 5a) and 10^{-15} m^2 (Fig. 5b). Results show that the fault

reactivation occurs at about 24 MPa for all the cases assuming the low initial fault permeability (Fig. 5a). Note that this reactivation pressure is slightly higher than the minimum principal stress at the same depth. The maximum pressure is reached within the first 200 days, with a value around 30 MPa for Case1 and Case3. Permeability changes along the fault zone become substantial and the pressure drops to around 22 MPa at the end of the 5 years of injection (Fig. 5a, green and red line). Case2, as explained earlier, features permeability changes only within the fault core, and very small changes occur in the damage zone. With a lower average permeability, the pressure potentially increases up to 40 MPa, i.e., an unrealistic value, at which point the simulation was terminated (Fig. 5a, black line).

The pressure evolution differs somewhat when considering a higher initial fault permeability of 10^{-15} m^2 (Fig. 5b). Reactivation always occurs at the same pressure, which is slightly higher than before (25 MPa). The maximum pressure may increase as much as 27 MPa (for Case1 and Case3) and 33 MPa (for Case2) after about 200 days of injection, only to decrease for all three cases to about 20 MPa at the end of the 5 years of injection (Fig. 5b).

Scenario 2

In this scenario, the fault zone is large and extensive (intersecting the entire 2 km thickness of the model) with an initial shear offset of 100 m, causing the multilayer system to be spatially shifted across the fault zone. For this reason, the central aquifer, where the CO_2 is injected, is hydraulically bounded on the right side by the shifted caprock. With the injection zone being hydraulically bounded, the pressure increases more rapidly for a given injection rate and the pressure might quickly exceed the minimum principle stress. Hence, we considered a smaller range of injection rates from 2 to 12 kg/s (which is still within the same order of magnitude as the injection at the In Salah CO_2 storage project—Shi et al., 2012; Rinaldi and Rutqvist, 2013).

Within this range of injection rates, it is very unlikely that a notable leakage would occur, and only for a very high fault initial permeability does some few percent (less than 8%) of the CO_2 leak into the upper aquifer (Figs. 6a and 6g). The explanation is that for low permeability, the CO_2 actually starts moving upward along the fault, but when it reaches the offset aquifer at the foot wall, the CO_2 migrates into this high-permeability aquifer rather than continuing upward by buoyancy (Figs. 6b and 6h). Some CO_2 migrates upward only for the case of a fault-zone permeability comparable to that of the aquifer permeability (Figs. 6c and 6i). In this scenario, injection pressure is generally much higher, since the injection reservoir is hydraulically bounded by the offset fault, and the higher pressure results in a greater permeability increase for Case1 and Case3. As shown in Figs. 6b and 6h, the permeability increases by as much as two orders of magnitude in the case of a relatively low initial fault permeability of 10^{-16} m^2. For a relatively high initial fault permeability of 10^{-14} m^2, the permeability increases are limited to less than one order of magnitude (Figs. 6c and 6i).

One small exception occurred for Case2 (Fig. 6d). As explained earlier for Scenario #1, when the permeability changes as a function of the volumetric strain, the permeability will change mostly within the fault core rather than within the damage zone. Then, when considering Case2 for Scenario #2 with low initial permeability within the fault zone (10^{-16} m^2), the fault core undergoes a very high permeability change (up to a 5-order-of-magnitude change after 1 year—Fig. 6e) compared to the surrounding damage zone, and the CO_2 will keep migrating upward along the fault core, as in a channel, and finally the CO_2 leaks into the upper aquifer (Fig. 6e). In the field, we may envision this channel developing at the interface between the fault core and the damage zone. Assuming a higher initial permeability for Case2 will then result in a leakage rate similar to Case1 and Case3 (Fig. 6f).

Much more interesting in this Scenario #2 is the relationship between magnitude of induced seismic events and leakage percentage (Fig. 7). Because of the scenario configuration (Fig. 2b), the hydraulically confined injection aquifer is easier to pressurize, and therefore seismicity can be triggered even for a smaller injection rate. For this scenario, we also found it notable that a seismic event might be produced even though the leakage rate is very low or null. For example, for all three simulated cases with low initial fault permeability (less than 10^{-15} m^2), events of magnitude in the range 2–3.5 are very likely, even without leakage into the upper aquifer. The results show basically no correlation between earthquake magnitude and leakage percentage. Rather, for most of the simulated cases in this scenario, a fault reactivation does not imply changes in permeability that would compromise the containment of the CO_2. This also means that in the case of a larger fault zone, the presence of seismic activity does not always imply a significant deterioration of caprock sealing properties. Again, the lack of correlation indicates that permeability changes do not affect the entire length of the fault; hence, the fault itself does not represent a preferential pathway for fluid to leak into the upper aquifer, within the range of simulated values.

In terms of seismic magnitude itself, the three cases show approximately the same values for all the different combinations, with reactivation occurring in most of the cases (except for cases with very high initial fault permeability and very low injection rate). Results also show events of greater magnitude for a lower injection rate. For example, in Case2, the event magnitude estimation for the simulation with injection rate of 4 kg/s and permeability of 10^{-15} m^2 is about 3.1 (Fig. 7f, black line), while for the same permeability, the simulation with 12 kg/s results in an event of magnitude 2.8 (Fig. 7f, green line). This effect may be explained in terms of timing: for

lower injection rates (4 kg/s), the system will require a longer time to increase the pressure up to the critical value for reactivation (384 days), and then the pressure itself has already been distributed much more extensively along the fault, producing at the time of reactivation a larger rupture compared to the case with higher injection rate (12 kg/s).

Fig. 8 shows an example of pressure evolution at the source for the three considered cases with injection rate 12 kg/s and with initial fault permeability of 10^{-16} m^2 (Fig. 8a) and 10^{-15} m^2 (Fig. 8b). The trend is different when compared to Scenario #1 (Fig. 5). First of all, the fault reactivation always occurs at a lower pressure (about 21 MPa for both permeabilities and for each case) and at a later time (about 100 days), indicating that the pressure has distributed more extensively along the fault, and a lower pressure is required for reactivation. Moreover, in this scenario, fluid pressurization occurs only on one side of the fault, leading to higher induced shear stress across the fault, which may also contribute to the lower pressure required for reactivation. For Case1 (green line in Fig. 8), after the reactivation, the pressure increases to reach a peak value after about 400 days, remaining at an approximately steady value until 1000 days, at which point an additional pressure increase occurs when CO_2 reaches the fault and starts to migrate upward and then laterally into the offset reservoir encountered in the foot wall of the fault (Fig. 6a and 6b). The same trend is observed for Case3, although with lower values. Case2 is the only case in which a substantial leakage occurs for both permeabilities (Fig. 6d). The CO_2 leakage into the upper aquifer results in a pressure drop of about 10 MPa for a low initial fault permeability of 10^{-16} m^2 and about 4 MPa for an initial fault permeability of 10^{-15} m^2. This drop in pressure in these cases is caused by the substantial (up to 5 orders of magnitude) permeability increase occurring along the fault core. Again, in the field, we may envision this as localized

shearing, creating a discrete open channel at the interface between the fault core and the damage zone.

DISCUSSION AND CONCLUSION

In this paper, we modeled the potential fault reactivation and CO_2 leakage through a fault zone during geological carbon sequestration activities in a series of different scenarios, including different geometries of the reservoir/caprock/fault system and different mechanical-dependent permeability laws. Specifically, we examined the short-term capability (i.e., during 5 years of active injection) of a fault zone to act as a pathway for upward migration of CO_2 by overpressure and buoyancy, and the potential for induced seismicity and seismic event magnitudes that could be triggered.

Our results show a poor correlation between seismic events and leakage, meaning that a single, relatively small-magnitude (between 2 and 3.5) event is not sufficient to substantially change the permeability along the entire fault length. Consequently, even if some changes in permeability would occur, the CO_2 does not migrate upward along the entire fault, and it may not break through the entire thickness of the caprock. Moreover, results also show that injecting at a low rate with a slow reservoir pressure increase does not imply less risk of inducing a seismic event, because the overpressure needed to trigger an event is always the same, independent of the injection rate or initial fault permeability.

We carried out a large number of simulations (about 200 simulations in total, i.e., 100 for each scenario) to determine how leakage rate and seismic magnitudes may be affected by injection

rates, fault permeability, and induced permeability changes for two different scenarios. The first scenario represented a minor, undetected fault zone (i.e., 1 km long) with no offset, while the second scenario represented a larger fault zone with an initial shear offset of 100 m.

For Scenario #1, results showed that a substantial amount of CO_2 may leak through the fault zone only in the case of a very high injection rate (more than 50 kg/s), or if the initial fault permeability were very high (10^{-14} m^2). Fault reactivation also occurred for high injection rates (more than 30 kg/s), especially when initial fault permeability is low (10^{-16} m^2).

For Scenario #2, results never showed substantial leakage, even though the injection-rate range was reduced to prevent an unrealistic pressurization of the aquifer. Most of the simulations performed never resulted in short-term CO_2 leakage into the upper aquifer, although the simulations showed that some few percentage of CO_2 (around 8%) may leak when the injection rate is high (12 kg/s) and the initial fault permeability is also high (10^{-14} m^2). Although no notable leakage occurred, most of the simulations in Scenario #2 were characterized by fault reactivation, producing seismic events of magnitude in the range of 2–3.5.

Consequently, our results show that a seismic reactivation may occur without significantly affecting the potential for leakage through a fault zone. This is also true for a small fault; a high injection rate is needed for reactivation, since permeability changes do not allow the pressure to accumulate. The seismic reactivation without leakage is more evident in Scenario #2, in which it is possible to simulate an induced earthquake even when using a relatively small injection rate.

Moreover, inclusion of rock heterogeneities (both mechanics and hydraulic properties) in the model will decrease the risk of leakage, and will help the CO_2 to be confined within the injection reservoir. Indeed, Jeanne et al. (2013b,c) demonstrated that for the same injection rate, fault length, and dip, as well as boundary and initial conditions, while the pressure increase is the same for homogeneous and heterogeneous models (hence producing the same fault slip), the amount of CO_2 leaking is definitely lower for a heterogeneous fault zone.

Note that while our model is the most current and comprehensive that we know of, it still includes a few approximations. The first (and probably the most important) is that we are only using a 2D model. Thus the question remains, what will change when considering a full 3D formulation? In theory, if the fault were not symmetric, the overpressure would be smaller and more distributed in space, and a higher injection rate would be necessary to reach the failure point. Moreover, complex 3D fault geometries, such as relay zones and step-overs, are not considered in this analysis. Step-overs and relays are likely to have a rate-limiting impact on the integrity of any CO_2 storage (e.g., Micklethwaite & Cox, 2004; Sheldon & Micklethwaite, 2007).

A second major approximation is that we can basically simulate only an induced event followed by mostly aseismic deformation. Thus, another question remains, will a series of notable (felt) earthquakes compromise the integrity of the system, allowing the fluids to move faster (and better) along the fault zone? However, in the field, if a felt seismic event occurs, the operators could reduce the injection rate to reduce the overpressure and try to avoid more seismic events. However, such action would not necessarily guarantee a cessation of events: at Basel, the biggest seismic event occurred after shutting down the injection.

As shown by Ingebritsen and Manning (2010), permeability of a seismically active region may reach very high values, which would favor the escape of the CO_2 through the fault zone. Especially in the case of high-magnitude aftershocks sequence, there were few indications of high permeability during natural events as high as 10^{-11} m^2 (e.g., during 1the 997 Umbria-Marche seismic sequence in Northern Italy – Miller et al., 2004) or even higher (e.g., Doby earthquake sequence, central Afar – Noir et al., 1997). However, during anthropogenic activity, such water disposal or geothermal stimulation, a 100-fold increase relative to pre-stimulation conditions was found, for example at Basel (Evans et al., 2005). Moreover, a review of ~90 cases by Talwani et al. (2007) showed that permeability in the regions experiencing injection-induced episodes is on the order of 10^{-15} – 10^{-13} m^2 at ~3 km depth. In our work, we considered permeabilities in the range proposed by Manning and Ingebritsen (1999) for an inactive crust, since injection should be performed in a safe zone (i.e., one that is not seismically active). We also found an appropriate 2-orders-magnitude increase in permeability, in agreement with observations (Evans et al., 2005; Talwani et al., 2007).

Finally, while the analyses presented in this paper serve as a baseline covering a range of scenarios and mechanisms, they still contain some limitations, including simplified 2D analysis of a 3D problem and the use of a simple slip-weakening fault rupture model with a fixed peak and residual strength (which can have a substantial effect on simulation results) For future analyses, a more complete rate-and-state formulation for fault friction evolution should be used to study the effects of multiple rupture events over long-term injections. Other aspects to be fully addressed are (1) the size of the reservoir and (2) the effects of a system with multiple caprocks and reservoirs.

ACKNOWLEDGMENTS

This work was supported by the Assistant Secretary for Fossil Energy, Office of Natural Gas and Petroleum Technology, through the National Energy Technology Laboratory, under the U.S. Department of Energy Contract No. DE-AC02-05CH11231. Technical review comments by Victor Vilarrasa at the Berkeley Lab, as well as editorial review by Dan Hawkes at the Berkeley Lab are all greatly appreciated. We would like to thank two anonymous reviewers for their thorough reviews and very useful comments.

REFERENCES

Bachmann, C. E., Wiemer, S., Woessner, J., Hainzl, S., 2011. Statistical analysis of the induced Basel 2006 earthquake sequence: Introducing a probability-based monitoring approach for Enhanced Geothermal Systems. *Geophys. J. Int.* 186(2). doi:10.1111/j.1365-246X.2011.05068.x.

Bandis, S. C., Lumsden, A. C., Barton, N. R., 1983. Fundamentals of rock joint deformation. *Int. J. Rock Mech. Mining Sci. Geomech. Abs.* 20(6), 249-368.

Beer, F. P., Johnson, E. R., 1992. *Mechanics of Materials*, McGraw-Hill, Inc, 2nd ed.

Ben-Zion, Y., Sammis, C. G., 2003. Characterization of fault zones, *Pure Appl. Geophys.*, 160, 677-715.

Birkholzer, J. T., Nicot, J. P., Oldenburg, C. M., Zhou, Q., Kraemer, S., Bandilla, K., 2011. Brine flow up a well caused by pressure perturbation from geological carbon sequestration: Static and dynamic evaluations. *Int. J. Greenh. Gas Control* 5(4), 850-861. doi:10.1016/j.ijggc.2011.01.003.

Cappa, F., Guglielmi, Y., Virieux, J., 2007. Stress and fluid transfer in a fault zone due to overpressures in the seismogenic crust, *Geophys. Res. Lett.*, 34, L05301. doi:10.1029/2006GL028980.

Cappa, F., Rutqvist, J., 2011a. Impact of CO_2 geological sequestration on the nucleation of earthquakes. *Geophys. Res. Lett.* 38, L17313. doi:10.1029/2011GL048487.

Cappa, F., Rutqvist, J., 2011b. Modeling of coupled deformation and permeability evolution during fault reactivation induced by deep underground injection of CO_2. *Int. J. Greenh. Gas Contr.* 5(2), 336-346. doi:10.1016/j.ijggc.2010.08.005.

Cappa, F., Rutqvist, J., 2012. Seismic rupture and ground accelerations induced by CO_2 injection in the shallow crust. *Geophys. J. Int.* 190, 1784-1789.

Chin, L. Y., Raghavan, R., Thomas, L. K., 2001. Fully coupled geomechanics and fluid-flow analysis of wells with stress-dependent permeability. *SPE Journal* 5, 32-45.

David, C., Wong T.-F., Zhu W., Zhang J., 1994. Laboratory measurement of compaction-induced permeability change in porous rock: Implications for the generation and maintenance of pore pressure excess in the crust, *Pure Appl. Geophys.*143, 425-456.

Davies, J. P., Davies, D. K., 2001. Stress-dependent permeability: characterization and modeling. *SPE Journal* 6, 224-235.

Evans, K. F., Genter, A., Sausse J., 2005. Permeability creation and damage due to massive injections into granite at 3.5 km at Soultz: 1. Borehole observations. *J. Geophys. Res.* 110, B04203, doi:10.1029/2004JB003168.

Faulkner, D. R., Mitchell, T. M., Healy, D., Heap, M., 2006. Slip on 'weak' faults by the rotation of regional stress in the fracture damage zone. *Nature* 444(7121), 922-925.

Faulkner, D. R., Rutter, E. H., 1998. The gas permeability of clay-bearing fault gouge at 20°C, In: *Faults, Fault Sealing and Fluid Flow in Hydrocarbon Reservoirs*, edited by G. Jones, Q. Fisher, and R.J. Knipe, Geol. Soc. Spec. Pub., 147-156.

Garagash, D. I., Germanovich, L. N., 2012. Nucleation and arrest of dynamic slip on a pressurized fault. *J. Geophys. Res.* 117(B10). doi:10.1029/2012JB009209.

Gudmundsson, A., 2000. Active fault zones and groundwater flow. *Geophys. Res. Lett.* 27(18), 2993-2996.

Gudmundsson, A., 2004. Effects of Young's modulus on fault displacement, *CR. Geosciences*, 336, 85-92.

Gudmundsson, A., Simmenes, T. H., Larsen, B., Philipp, S. L., 2010. Effects of internal structure and local stresses on fracture propagation, deflection, and arrest in fault zones, *J. Struct. Geol.*, (in press), doi: 10.1016/j.jsg.2009.08.013.

Guglielmi, Y., Cappa, F., Amitrano, D., 2008. High-definition analysis of fluid-induced seismicity related to the mesoscale hydromechanical properties of a fault zone, *Geophys. Res. Lett.*, *35*, L06306. doi:10.1029/2007GL033087.

Hepple, R.P., Benson, S.M., 2005. Geologic storage of carbon dioxide as a climate change mitigation strategy: performance requirements and the implications of surface seepage. *Environ. Geol.* 47(4), 576-585.

Hou, Z., Rockhold, M. L., Murray, C.J., 2012. Evaluating the impact of caprock and reservoir properties on potential risk of CO_2 leakage after injection. *Environ. Earth Sci.* 66, 2403-2415. doi:10.1007/s12665-011-1465-2.

Hsiung, S. M., Chowdhury, A. H., Nataraja, M. S., 2005. Numerical simulation of thermal-mechanical processes observed at the Drift-Scale Heater Test at Yucca Mountain, Nevada, USA. *Int. J. Rock Mech. Min. Sci.* 42(5-6), 652-666. doi:10.1016/j.ijrmms.2005.03.006.

Ingebritsen, S. E., Manning, C. E., 2010. Permeability of the continental crust: dynamic variations inferred from seismicity and metamorphism. *Geofluids* 10, 193-205. Doi: 10.1111/j.1468-8123.2010.00278.x.

ITASCA, 2009. FLAC3d v4.0, Fast Lagrangian Analysis of Continua in 3 Dimensions, User's Guide. Itasca Consulting Group, Minneapolis, MN, USA.

Jaeger, J. C., Cook, N., 1979. Fundamentals of Rock Mechanics. Third ed. Chapman & Hall, New York, pp. 28-30.

Jeanne P., Guglielmi Y, Lamarche J., Cappa F., Marié L., 2012a. Architectural characteristics and petrophysical properties evolution of a strike-slip fault zone in a fractured porous carbonate reservoir. *J. Struct. Geol.*, 44, 93-109. doi: 10.1016/j.jsg.2012.08.016

Jeanne P., Guglielmi Y., and Cappa F., 2012b. Multiscale seismic signature of a small fault zone in carbonate reservoir: Relationships between V_P Imaging, fault zone architecture and cohesion. *Tectonophysics*, doi:10.1016/j.tecto.2012.05.012, 554-557 (2012) 185–201.

Jeanne, P., Guglielmi Y., and Cappa. F., 2013a. Dissimilar properties within a carbonate-reservoir's small fault zone, and their impact on the pressurization and leakage associated with CO_2 injection. *J. Struct. Geol.*, 47, 25-35, doi:10.1016/j.jsg.2012.10.010

Jeanne P., Guglielmi Y., Cappa F., 2013b. Hydromechanical heterogeneities of mature fault zones : impacts on fluid flow. *Ground Water*, doi : 10.1111/gwat.12017

Jeanne, P., Rinaldi, A. P., Rutqvist, J., Cappa, F., Guglielmi, Y., 2013c. Relation between fault zone architecture, earthquake magnitude and leakage associated with CO_2 injection in a multilayered sedimentary system, in: Proceedings of the 47th US Rock Mechanics, Geomechanics Symposium. San Francisco, 23 26 June 2013.

Kanamori, H., Anderson, D. L., 1975. Theoretical basis of some empirical relations in seismology. *Bull. Seism. Soc. Am.* 65(5), 1073-1095.

Kanamori, H., Brodsky, E. E., 2004. The physics of earthquakes. *Rep. Prog. Phys.* 67(8), 1429. doi:10.1088/0034-4885/67/8/R03.

Kerr, R. A., 2012. Learning how to NOT make your own Earthquakes. *Science* 335(6075). doi:10.1126/science.335.6075.1436.

Leclère, H., Fabbri, O., Daniel, G., Cappa, F., 2012. Reactivation of a strike-slip fault by fluid overpressuring in the southwestern french-italian alps. *Geophys. J. Int.* 189(1), 29-37.

Leverett, M. C., 1941. Capillary behavior in porous media. *Trans. Am. Inst. Mining Eng.* 142, 341-358.

Manga, M., Beresnev, I., Brodsky, E. E., Elkhoury, J. E., Elsworth, D., Ingebritsen, S. E., Mays, D. C., Wang, C.-Y., 2012. Changes in permeability caused by transient stress: field observations, experiments, and mechanisms. *Rev. Geophys.* 50, RG2004. doi: 10.1029/2011RG000382.

Manning, C. E., Ingebritsen, S. E., 1999. Permeability of the continental crust: the implications of geothermal data and metamorphic systems. *Review of Geophysics* 37, 127-150. doi: 10.1029/1998RG900002.

Mazzoldi, A., Rinaldi, A. P., Borgia, A., Rutqvist, J., 2012. Induced seismicity within geological carbon sequestration projects: Maximum earthquake magnitude and leakage potential from undetected faults. *Int. J. Greenh. Gas Control* 10, 434-442. doi:10.1016/j.ijggc.2012.07.012.

Micklethwaite, S., Cox, S. F., 2004. Fault-segment rupture, aftershock-zone fluid flow, and mineralization. *Geology* 32, 813-816. doi: 10.1130/G20559.1.

Miller, S., Collettini, C., Chiaroluce, L., Cocco, M., Barchi, M., Kaus, B. J. P., 2004. Aftershocks driven by high-pressure CO_2 source at depth. *Nature* 427, 724-727. doi: 10.1038/nature02251.

Mitchell, T. M., Faulkner, D. R., 2009. The nature and origin of off-fault damage surrounding strike-slip fault zones with a wide range of displacements: a field study from the Atacama fault system, northern Chile, *J. Struct. Geol.*, 31(8), 802-816. doi:10.1016/j.jsg.2009.05.002.

Myer, L. R., Daley, T., 2011. Elements of a best practices approach to induced seismicity in geologic storage. *Energy Procedia* 4, 3707-3713.

National Research Council, 2012. Induced seismicity potential in energy technologies, *National Academies Press*, Washington D.C., pp. 300.

Nicol, A., Come, R., Gerstenberger, M., Christophersen, A., 2011. Induced seismicity and its implications for CO_2 storage risk. *Energy Procedia* 4, 3699-3706.

Nicot, J. P., 2008. Evaluation of large-scale CO_2 storage on fresh-water sections of aquifers: an example from Texas Gulf Coast Basin. *Int. J. Greenh. Gas Control* 2(4), 582-593. doi:10.106/j/ijggc.2008.03.004.

Nicot, J. P., Oldenburg, C. M., Houseworth, J. E., Choi, J. W., 2013. Analysis of potential leakage pathways at the Cranfield, MS, U.S.A., CO_2 sequestration site. *Int. J. Greenh. Gas Contr.* 18, 388-400. doi:10.1016/j.ijggc.2012.10.011.

Noir, J., Jacques, E., Békri, S., Adler, P. M., Tapponnier, O., King, G. C. P., 1997. Fluid flow triggered migration of events in the 1989 Dobi earthquake sequence of Central Afar. *Geophys. Res. Lett.* 24(18), 2336-2338.

Oldenburg, C. M., Rinaldi, A. P., 2011. Buoyancy Effects on Upward Brine Displacement Caused by CO_2 Injection. *Transp. Porous Med.* 87, 525-540. doi:10.1007/s11242-010-9699-0.

Pacala, S., Socolow, R., 2004. Stabilization wedges: solving the climate problem for the next 50 years with current technologies. *Science* 13305(5686), 968-972.

Pruess, K., Oldenburg, C. M., Moridis, G., 2011. *TOUGH2 User's Guide*, Version 2.1. Paper LBNL-43134 (revised). Lawrence Berkeley Natl. Lab., Berkeley, CA, USA.

Pruess, K., 2005. *ECO2N: A TOUGH2 Fluid Property Module for Mixtures of Water, NaCl, and CO_2*. Paper LBNL- 57952. Lawrence Berkeley Natl. Lab., Berkeley, CA, USA.

Rinaldi, A. P., Rutqvist, J., 2013. Modeling of deep fracture zone opening and transient ground surface uplift at KB-502 CO_2 injection well, In Salah, Algeria. *Int. J. Greenh. Gas. Contr.* 12, 155-167.

Rinaldi, A. P., Rutqvist, J., Sonnenthal, E. L., Cladouhos, T. T., 2013. Coupled THM modeling of hydroshearing stimulation in tight fractured volcanic rock. *Transp. Porous Med.*, submitted.

Rutqvist, J., 2011. Status of TOUGH-FLAC simulator and recent applications related to coupled fluid flow and crustal deformations. *Comput. Geosci.* 37, 739-750.

Rutqvist, J., 2012. The Geomechanics of CO_2 Storage in Deep Sedimentary Formation. *Geotech. Geol. Eng.* 30(3), 525-551. doi:10.1007/s10706-011-9491-0.

Rutqvist, J., Birkholzer, J., Cappa, F., Tsang, C.-F., 2007. Estimating maximum sustainable injection pressure during geological sequestration of CO_2 using coupled fluid flow and geomechanical fault-slip analysis. *Energy Conversion and Management* 48, 1798–1807. doi:10.1016/j.enconman.2007.01.021

Rutqvist, J., P. F. Dobson, J. Garcia, C. Hartline, P. Jeanne, C. M. Oldenburg, D. W. Vasco, M. Walters, 2013a. The Northwest Geysers EGS Demonstration Project, California: Pre-stimulation Modeling and Interpretation of the Stimulation. *Mathematical Geosciences*, Online First. doi: 10.1007/s11004-013-9493-y.

Rutqvist, J., Kim, H. M., Ryu, D. W., Synn, J. H., Song, W. K., 2012a. Modeling of coupled thermodynamic and geomechanical performance of underground compressed air energy storage in lined rock caverns. *Int. J. Rock Mech. & Min. Sci.* 52, 71-81. doi:10.1016/j.ijrmms.2012.02.010.

Rutqvist, J., Liu, H. H., Vasco, D. W., Pan, L., Kappler, K., Majer, E., 2011. Coupled non-isothermal, multiphase fluid flow, and geomechanical modeling of ground surface deformations and potential for induced micro-seismicity at the In Salah CO_2 storage operation. *Energy Procedia* 4, 3542-3549. doi:10.1016/j.egypro.2011.02.282.

Rutqvist, J., Moridis, G., Grover, T., Silpngarmlert, S., Collett, T., Holdich, S., 2012b. Coupled multiphase fluid flow and wellbore stability analysis associated with gas production from

oceanic hydrate-bearing sediments. *J. Petrol. Sci. Eng.* 92-93, 65-81. doi:10.1016/j.petrol.2012.06.004.

Rutqvist, J., Rinaldi, A. P., Cappa, F., Moridis, G. J., 2013b. Modeling of fault reactivation and induced seismicity during hydraulic fracturing of Shale-Gas reservoir. *J. Petrol. Sci. Eng.* 107, 31-44. doi:10.1016/j.petrol.2013.04.023

Rutqvist, J., Stephansson, O., 2003. The role of hydromechanical coupling in fractured rock engineering. *Hydrogeology Journal* 11(1), 7-40.

Rutqvist, J., Tsang, C.-F., 2002. A study of caprock hydromechanical changes associated with CO_2-injection into a brine formation. *Environ. Geol.* 42, 296-305. doi:10.1007/s00254-001-0499-2.

Rutqvist, J., Tsang, C.-F., 2012. Multiphysics processes in partially saturated fractured rock: Experiments and models from yucca mountain. *Rev. Geophys.* 50(3). doi:10.1029/2012RG000391.

Rutqvist, J., Vasco, D. W., Myer, L., 2010. Coupled reservoir-geomechanical analysis of CO_2 injection and ground deformations at In Salah, Algeria. *Int. J. Greenh. Gas Control* 4, 225-230. doi:10.1016/j.ijggc.2009.10.017.

Rutqvist, J., Wu, Y. S., Tsang, C.-F., Bodvarsson, G., 2002. A modeling approach for analysis of coupled multiphase fluid flow, heat transfer, and deformation in fractured porous rock. *Int. J. Rock Mech. Min. Sci.* 39, 429-442.

Shapiro, S. A., Dinske, C., 2009. Scaling of seismicity induced by nonlinear fluid-rock interaction. *J. Geophys. Res.* 114(B09307). doi:10.1029/2008JB006145.

Sheldon, H. A., Micklethwaite, S., 2007. Damage and permeability around faults: Implications and mineralization. *Geology* 35, 903-906. doi: 10.1130/G23860A.1.

Shi, J. Q., Sinayuc, C., Durucan, S., Korre, A., 2012. Assessment of carbon dioxide plume behaviour within the storage reservoir and the lower caprock around the KB-502 injection well at In Salah. *Int. J. Greenh. Gas. Control* 7, 115-126. doi:10.1016/j.jiggc.2012.01.002.

Sibson, R. H., 1990. Conditions for fault-valve behaviour. *Geological Society, London, Special Publications* 54, 12-28. doi:10.1144/gsl.sp.1990.054.01.02.

Sibson, R. H., 2003. Thickness of the seismic slip zone, *Bull. Seism. Soc. Am.*, 93(3), 1169-1178.

Talwani, P., Chen, L., Gahalaut, K., 2007. Seismogenic permeability, k_s. *J. Geophys. Res.* 112, B07309. Doi:10.1029/2006JB004665.

Terakawa, T., Miller, S. A., Deichmann, N., 2012. High fluid pressure and triggered earthquakes in the enhanced geothermal system in Basel, Switzerland. *J. Geophys. Res.* 117(B7). doi:10.1029/2011JB008980.

Terzaghi, K., 1923. Die Berechning deer Durchlassigkeitziffer des Tonesaus dem Verlauf Spannungserscheinungen, Akad. Der Wissenchafen in Wien, Sitzungsberichte, Mathematisch-naturwissenschafttliche Klasse. Part lia 142(3/4), 125-138.

Todesco, M., Rutqvist, J., Chiodini, G., Pruess, K., Oldenburg, C. M., 2004. Modeling of recent volcanic episodes at Phlegrean Fields (Italy): geochemical variations and ground deformation. *Geothermics* 33, 531-547. doi:10.1016/j.geothermics.2003.08.014.

van Genuchten, M. T., 1980. A closed form equation for predicting the hydraulic conductivity of unsaturated soils. *Soil Sci. Soc. Am. J.* 44, 892-898.

Vermilye, J. M., and Scholz, C. H., 1998. The process zone: A microstructural view of fault growth, *J. Geophys. Res.*, 103(B6), 12,223–12,237.

Vilarrasa, V., Bolster, D., Olivella, S., Carrera, J., 2010. Coupled hydromechanical modeling of CO_2 sequestration in deep saline aquifers. *Int. J. Greenh. Gas Control* 4(6), 910-919. doi:10.1016/j.ijggc.2010.06.006.

Wibberley, C. A., Shimamoto, J., 2003. T., Internal structure and permeability of major strike-slip fault zones: the Median Tectoni Line in Mie Prefecture, Southwest Japan, *J. Struct. Geol.*, 25:59-78.

Wilson, J. E., Chester, J. S., Chester, F. M., 2003. Microfracture analysis of fault growth and wear processes, Punchbowl Fault, San Andreas System, California, *J. Struct. Geol.*, 25(11), 1855-1873.

Zhou, R., Huang, L., Rutledge, J., 2010. Microseismic event location for monitoring CO_2 injection using double-difference tomography. *Lead. Edge* 29, 201-214.

Zoback, M. D., Gorelick, S. M., 2012. Earthquake triggering and large-scale geologic storage of carbon dioxide. *Proceedings of the National Academy of Sciences*. doi:10.1073/pnas.1202473109.

Tables

Table 1. Mechanical and hydraulic properties used in the numerical modeling for both scenarios #1 and #2 for each domain. Listed porosity and permeability for the fault zone represent the initial non-stressed value (after Cappa and Rutqvist, 2011a).

Layer	Upper Aquifer	Central Aquifer	Basal Aquifer	Caprock	Fault
Young's modulus, E (GPa)	10	10	10	10	5
Poisson's ratio, ν (-)	0.25	0.25	0.25	0.25	0.25
Rock density, ρ (kg/m^3)	2260	2260	2260	2260	2260
Peak friction angle, φ ($^\circ$)	-	-	-	-	31
Residual friction angle, φ ($^\circ$)	-	-	-	-	11
Dilation angle, ψ ($^\circ$)	-	-	-	-	10
Porosity, φ (%)	10	10	1	1	10
Permeability, κ (m^2)	10^{-14}	10^{-13}	10^{-16}	10^{-19}	10^{-16} - 10^{-14}
Residual CO_2 saturation (-)	0.05	0.05	0.05	0.05	0.05
Residual liquid saturation (-)	0.3	0.3	0.3	0.3	0.3
Van Genuchten (1980), p_0 (kPa)	19.9	19.9	621	621	19.9
Van Genuchten (1980), m (-)	0.457	0.457	0.457	0.457	0.457

Figures captions

Figure 1. (a) Sketch of a normal fault illustrating the geometrical and mechanical variables used to estimate the seismic moment (M_0) (L = fault length, W = fault width, A = ruptured area (grey dashed zone), d = final fault displacement, μ = shear modulus of the crust). (b) Close-up view of the typical internal structure of a fault zone, from the core zone through the intensively fractured damage zone and the less fractured transition zone to the unfractured host rock.

Figure 2. Simulated scenarios with initial and boundary conditions. (a) Configuration for an undetected fault, 1 km long with no offset. (Mazzoldi et al., 2012). Figure also shows the orientation of the considered stress in this 2D models; (b) Configuration for a long fault, with 100 m offset and extending for the entire 2 km domain (Cappa and Rutqvist, 2011a,b, 2012).

Figure 3. Percentage of CO_2 leaking into the upper aquifer as a function of fault permeability and injection rate for a 1 km-long fault with no offset, and resulting plume and permeability increase for single simulation with injection rate 20 kg/s and initial fault permeability 10^{-16} m^2, and injection rate 100 kg/s and initial fault permeability 10^{-14} m^2 (a, b, c) Case1: fault permeability changes calculated as function of mean stress. (d, e, f) Case2: fault permeability changes calculated as a function of the volumetric strain. The white contour in figure d indicates the region where the injection pressure exceeded 35 MPa. (g, h, i) Case3: fault permeability changes calculated as a function of both fault normal stress and plastic shear and tensile strain.

Figure 4. Magnitude of a single event due to a sudden slip along the 1 km-long fault zone with no offset as a function of initial fault permeability and injection rate, and resulting displacement for single simulation with injection rate 20 kg/s (black line), 50 kg/s (red line) and 100 kg/s (black line), and initial fault permeability 10^{-16} m^2 and 10^{-15} m^2 (a, b, c) Case1: fault permeability changes calculated as function of mean stress. (d, e, f) Case2: fault permeability changes

calculated as a function of the volumetric strain. (g, h, i) Case3: fault permeability changes calculated as a function of both fault normal stress and plastic shear and tensile strain.

Figure 5. Example of pressure evolution at the injection point for the 1 km-long fault zone with no initial shear offset. (a) injection rate 100 kg/s and initial fault permeability 10^{-16} m^2 and (b) injection rate 100 kg/s and initial fault permeability 10^{-15} m^2 for the three different cases: Case1 (green line), Case2 (black line), and Case3 (red line). The "star" symbol corresponds to the rapid response to injection, the "point" symbol corresponds to the pressure peak, and the "square" symbol correspond the pressure at the end of our injection scenario (i.e. 5 years).

Figure 6. Percentage of CO_2 leaking into the upper aquifer as a function of permeability and injection rate for a long fault (length greater than 2 km) with 100 m initial shear offset, and resulting plume and permeability increase for single simulation with injection rate 12 kg/s, and initial fault permeability 10^{-16} m^2 and 10^{-14} m^2. (a, b, c) Case1: fault permeability changes calculated as function of mean stress. (d, e, f) Case2: fault permeability changes calculated as a function of the volumetric strain. (g, h, i) Case3: fault permeability changes calculated as a function of both fault normal stress and plastic shear and tensile strain.

Figure 7. Magnitude of a single event due to a sudden slip along the 1 km-long fault zone with no offset as a function of initial fault permeability and injection rate, and resulting displacement for single simulation with injection rate 4 kg/s (black line), 8 kg/s (red line) and 12 kg/s (black line), and initial fault permeability 10^{-16} m^2 and 10^{-15} m^2 (a, b, c) Case1: fault permeability changes calculated as function of mean stress. (d, e, f) Case2: fault permeability changes calculated as a function of the volumetric strain. (g, h, i) Case3: fault permeability changes calculated as a function of both fault normal stress and plastic shear and tensile strain.

Figure 8. Example of pressure evolution at the injection point for the long fault zone (length greater than 2 km) with a 100 m initial shear offset. (a) injection rate 12 kg/s and initial fault

permeability 10^{-16} m^2 and (b) injection rate 12 kg/s and initial fault permeability 10^{-15} m^2 for the three different cases: Case1 (green line), Case2 (black line), and Case3 (red line). The "star" symbol corresponds to the rapid response to injection, the "point" symbol corresponds to the pressure peak, and the "square" symbol correspond the pressure at the end of our injection scenario (i.e. 5 years).

Figure 1

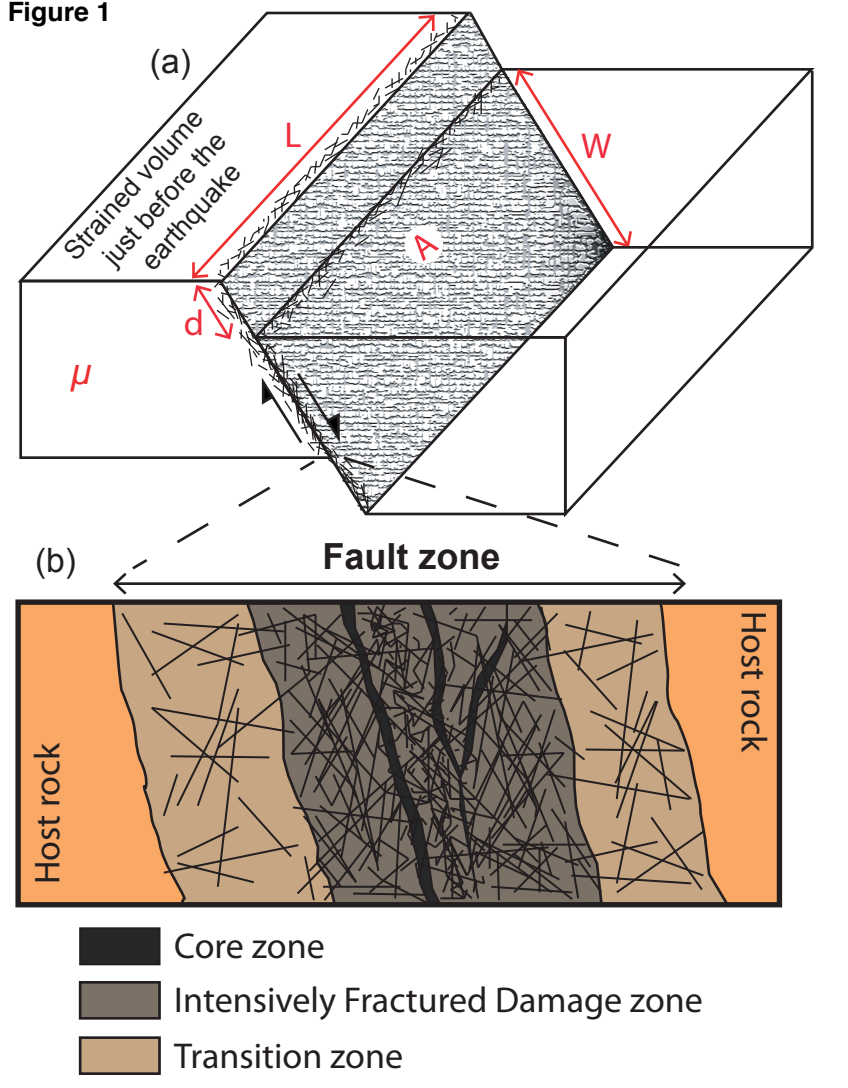
(a)
Strained volume just before the earthquake
L
W
A
d
μ
(b)
Fault zone
Host rock
Host rock
Core zone
Intensively Fractured Damage zone
Transition zone

Figure 2

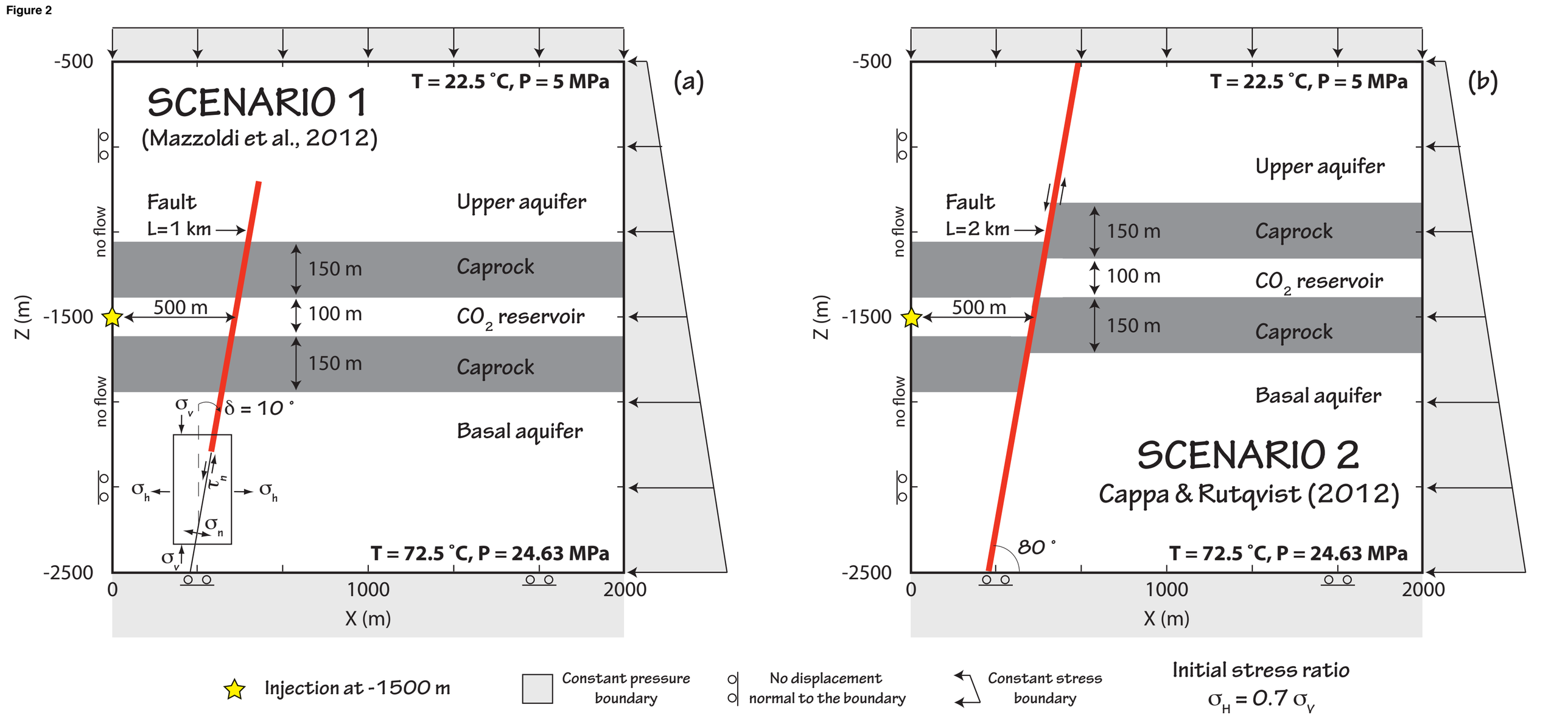
SCENARIO 1
(Mazzoldi et al., 2012)
T = 22.5 °C, P = 5 MPa
(a)
Fault
L=1 km
Upper aquifer
150 m
Caprock
500 m
100 m
CO2 reservoir
150 m
Caprock
no flow
no flow
δ = 10 °
Basal aquifer
σv
σh
σh
τn
σn
σv
T = 72.5 °C, P = 24.63 MPa
Z (m)
-500
-1500
-2500
0
1000
2000
X (m)
(b)
T = 22.5 °C, P = 5 MPa
Upper aquifer
Fault
L=2 km
150 m
Caprock
100 m
CO2 reservoir
500 m
150 m
Caprock
Basal aquifer
SCENARIO 2
Cappa & Rutqvist (2012)
80 °
T = 72.5 °C, P = 24.63 MPa
Injection at -1500 m
Constant pressure boundary
No displacement normal to the boundary
Constant stress boundary
Initial stress ratio
σH = 0.7 σV

Figure 3

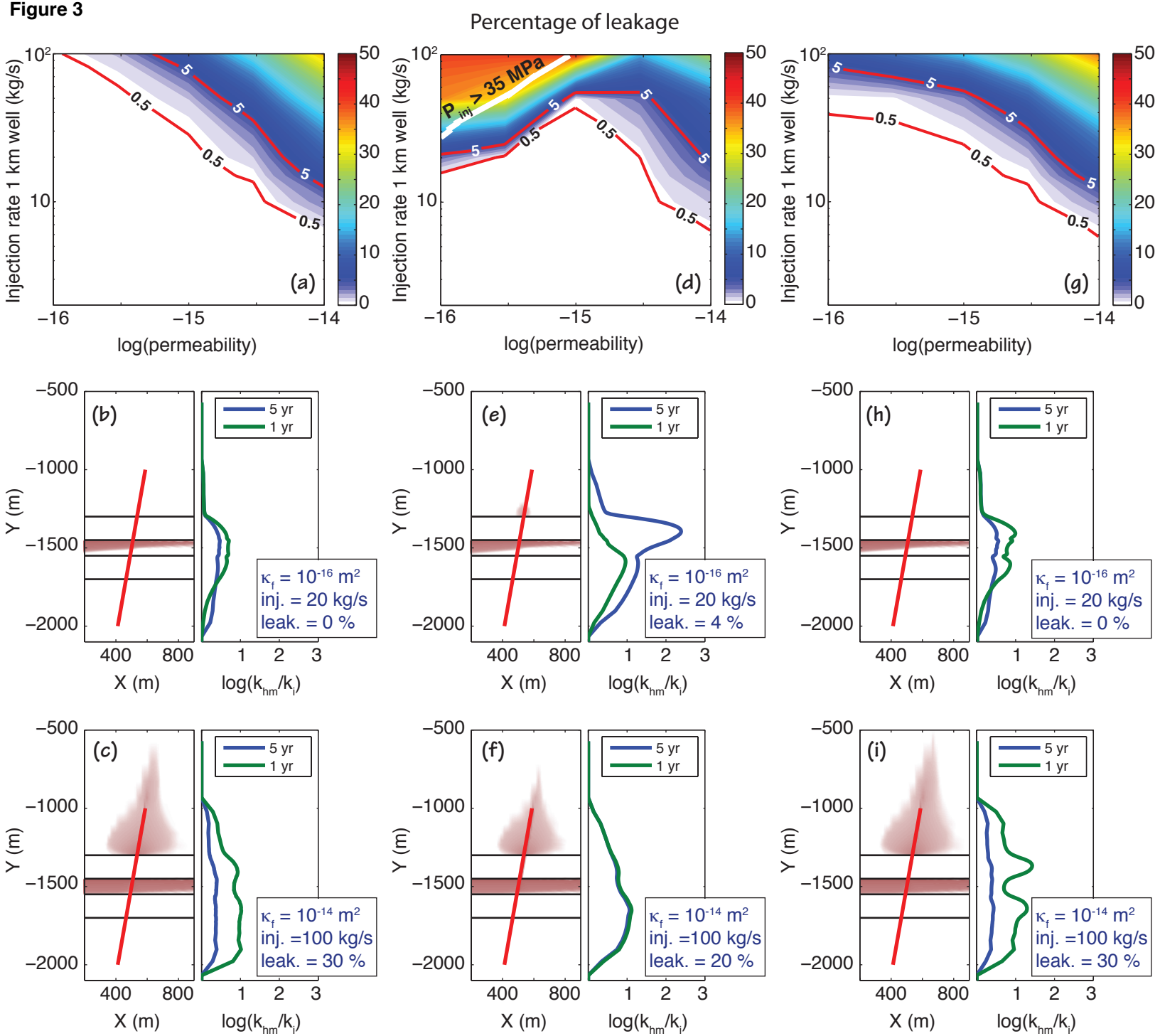
Percentage of leakage
Injection rate 1 km well (kg/s)
log(permeability)
(a)
(d)
(g)
P inj > 35 MPa
(b)
(e)
(h)
(c)
(f)
(i)
Y (m)
X (m)
log(khm/ki)
5 yr
1 yr
κf = 10-16 m2
inj. = 20 kg/s
leak. = 0 %
κf = 10-16 m2
inj. = 20 kg/s
leak. = 4 %
κf = 10-16 m2
inj. = 20 kg/s
leak. = 0 %
κf = 10-14 m2
inj. =100 kg/s
leak. = 30 %
κf = 10-14 m2
inj. =100 kg/s
leak. = 20 %
κf = 10-14 m2
inj. =100 kg/s
leak. = 30 %

Figure 4

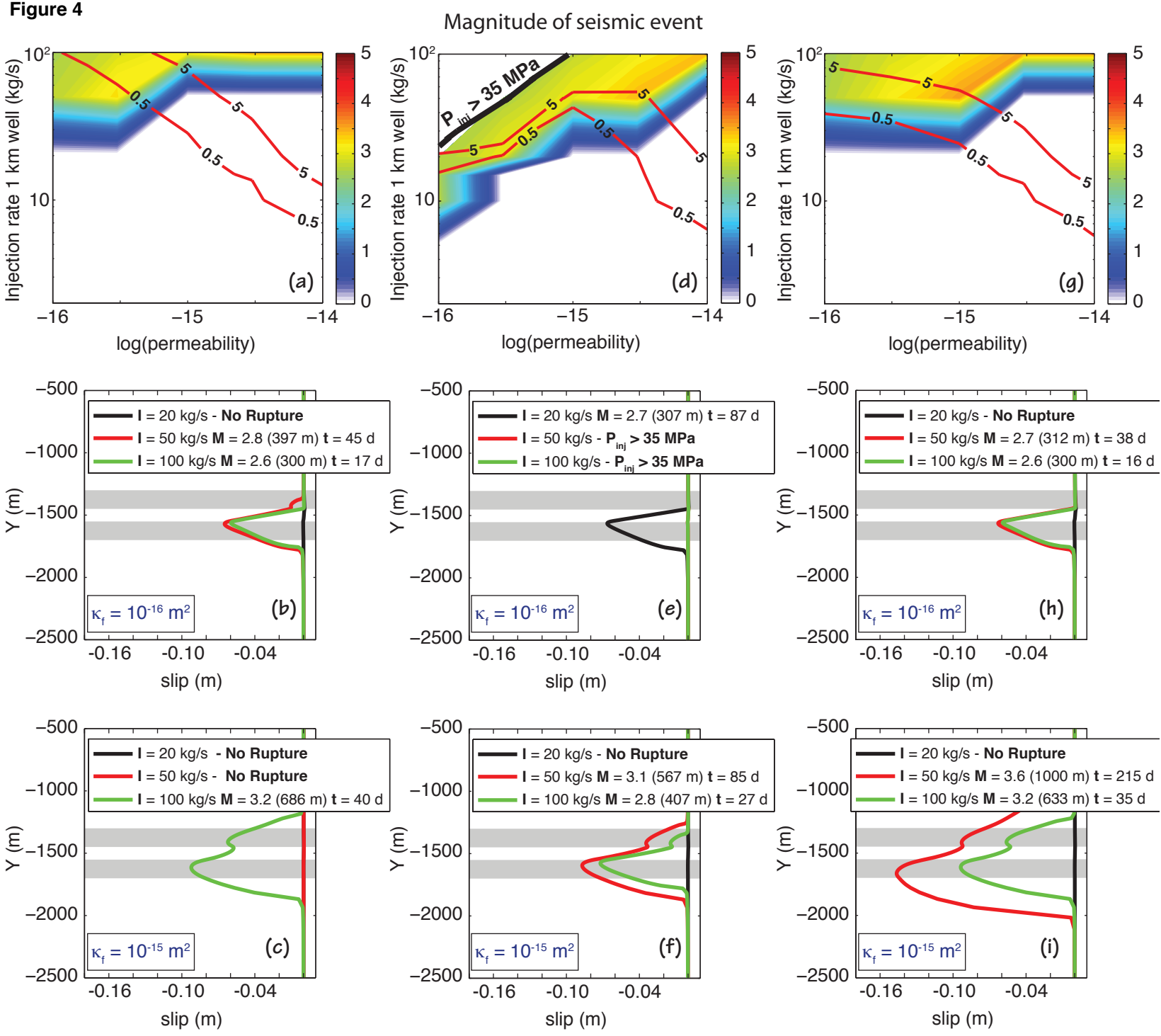
Magnitude of seismic event
Injection rate 1 km well (kg/s)
log(permeability)
P_{inj} > 35 MPa
(a)
(d)
(g)
Y (m)
slip (m)
I = 20 kg/s - No Rupture
I = 50 kg/s M = 2.8 (397 m) t = 45 d
I = 100 kg/s M = 2.6 (300 m) t = 17 d
I = 20 kg/s M = 2.7 (307 m) t = 87 d
I = 50 kg/s - P_{inj} > 35 MPa
I = 100 kg/s - P_{inj} > 35 MPa
I = 20 kg/s - No Rupture
I = 50 kg/s M = 2.7 (312 m) t = 38 d
I = 100 kg/s M = 2.6 (300 m) t = 16 d
I = 20 kg/s - No Rupture
I = 50 kg/s - No Rupture
I = 100 kg/s M = 3.2 (686 m) t = 40 d
I = 20 kg/s - No Rupture
I = 50 kg/s M = 3.1 (567 m) t = 85 d
I = 100 kg/s M = 2.8 (407 m) t = 27 d
I = 20 kg/s - No Rupture
I = 50 kg/s M = 3.6 (1000 m) t = 215 d
I = 100 kg/s M = 3.2 (633 m) t = 35 d
$\kappa_f = 10^{-16}$ m^2
$\kappa_f = 10^{-15}$ m^2
(b)
(c)
(e)
(f)
(h)
(i)

Figure 5

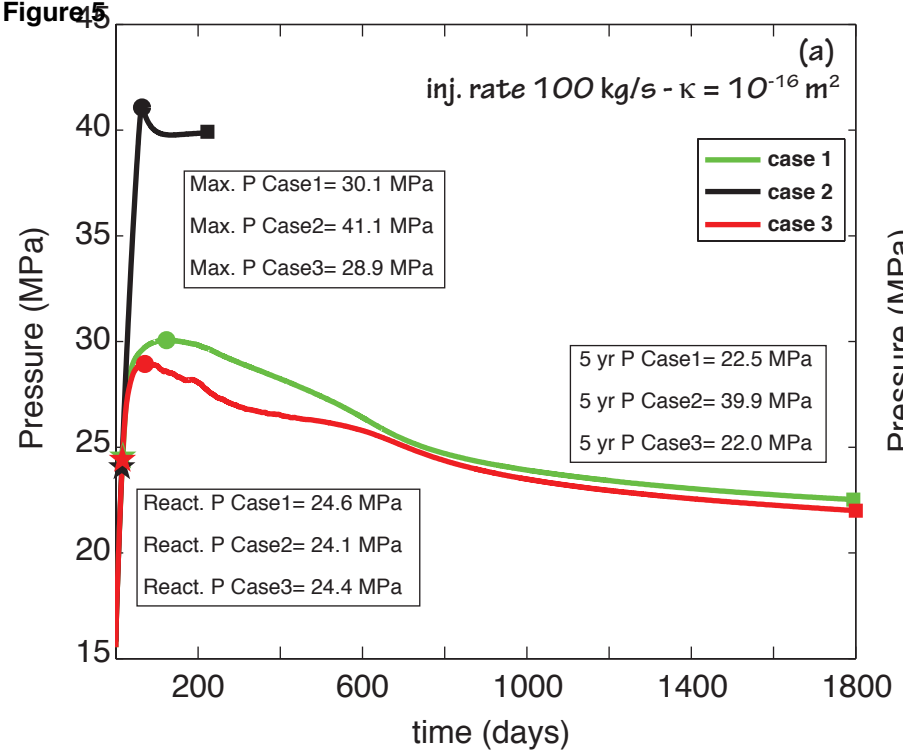
(a)
inj. rate 100 kg/s - κ = 10^-16 m^2
case 1
case 2
case 3
Max. P Case1= 30.1 MPa
Max. P Case2= 41.1 MPa
Max. P Case3= 28.9 MPa
5 yr P Case1= 22.5 MPa
5 yr P Case2= 39.9 MPa
5 yr P Case3= 22.0 MPa
React. P Case1= 24.6 MPa
React. P Case2= 24.1 MPa
React. P Case3= 24.4 MPa
Pressure (MPa)
time (days)
15
20
25
30
35
40
45
200
600
1000
1400
1800

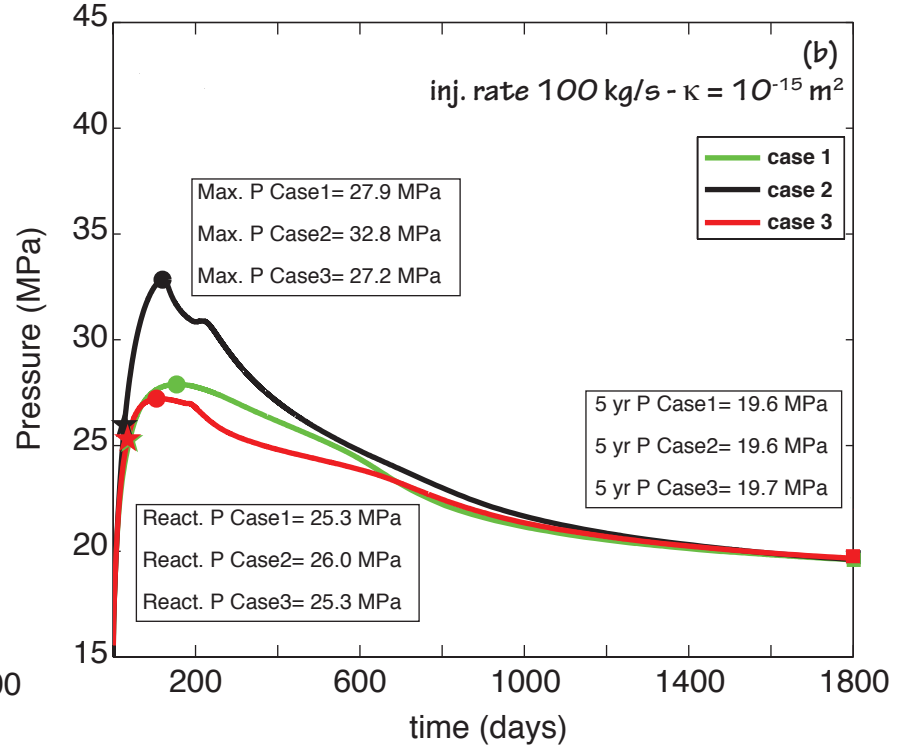
(b)
inj. rate 100 kg/s - κ = 10^-15 m^2
case 1
case 2
case 3
Max. P Case1= 27.9 MPa
Max. P Case2= 32.8 MPa
Max. P Case3= 27.2 MPa
5 yr P Case1= 19.6 MPa
5 yr P Case2= 19.6 MPa
5 yr P Case3= 19.7 MPa
React. P Case1= 25.3 MPa
React. P Case2= 26.0 MPa
React. P Case3= 25.3 MPa
Pressure (MPa)
time (days)
15
20
25
30
35
40
45
200
600
1000
1400
1800

Figure 6

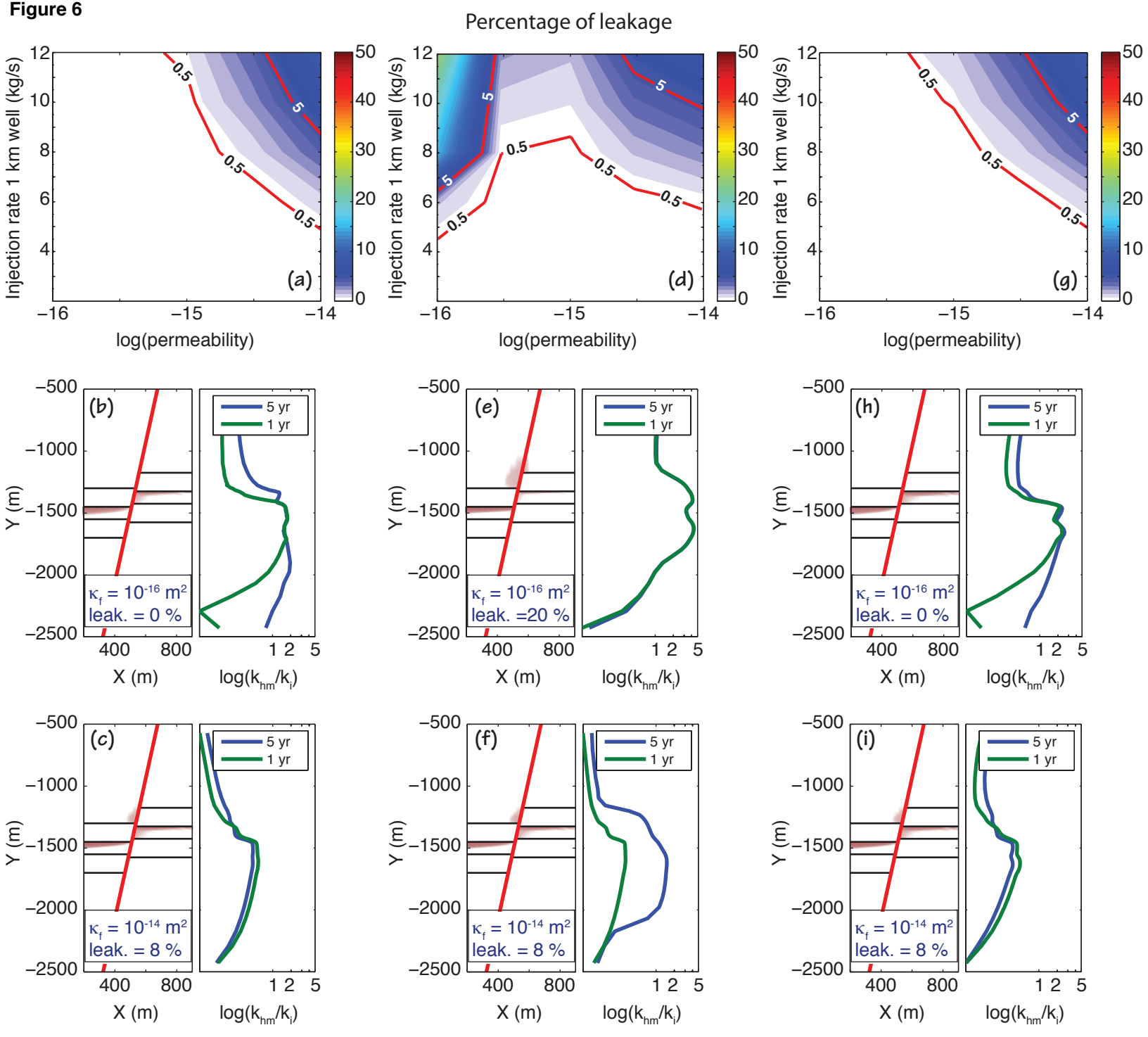
Percentage of leakage
Injection rate 1 km well (kg/s)
log(permeability)
(a)
(d)
(g)
(b)
(e)
(h)
(c)
(f)
(i)
Y (m)
X (m)
log(k_hm/k_i)
5 yr
1 yr
κ_f = 10^-16 m^2
leak. = 0 %
leak. =20 %
κ_f = 10^-14 m^2
leak. = 8 %

Figure 7

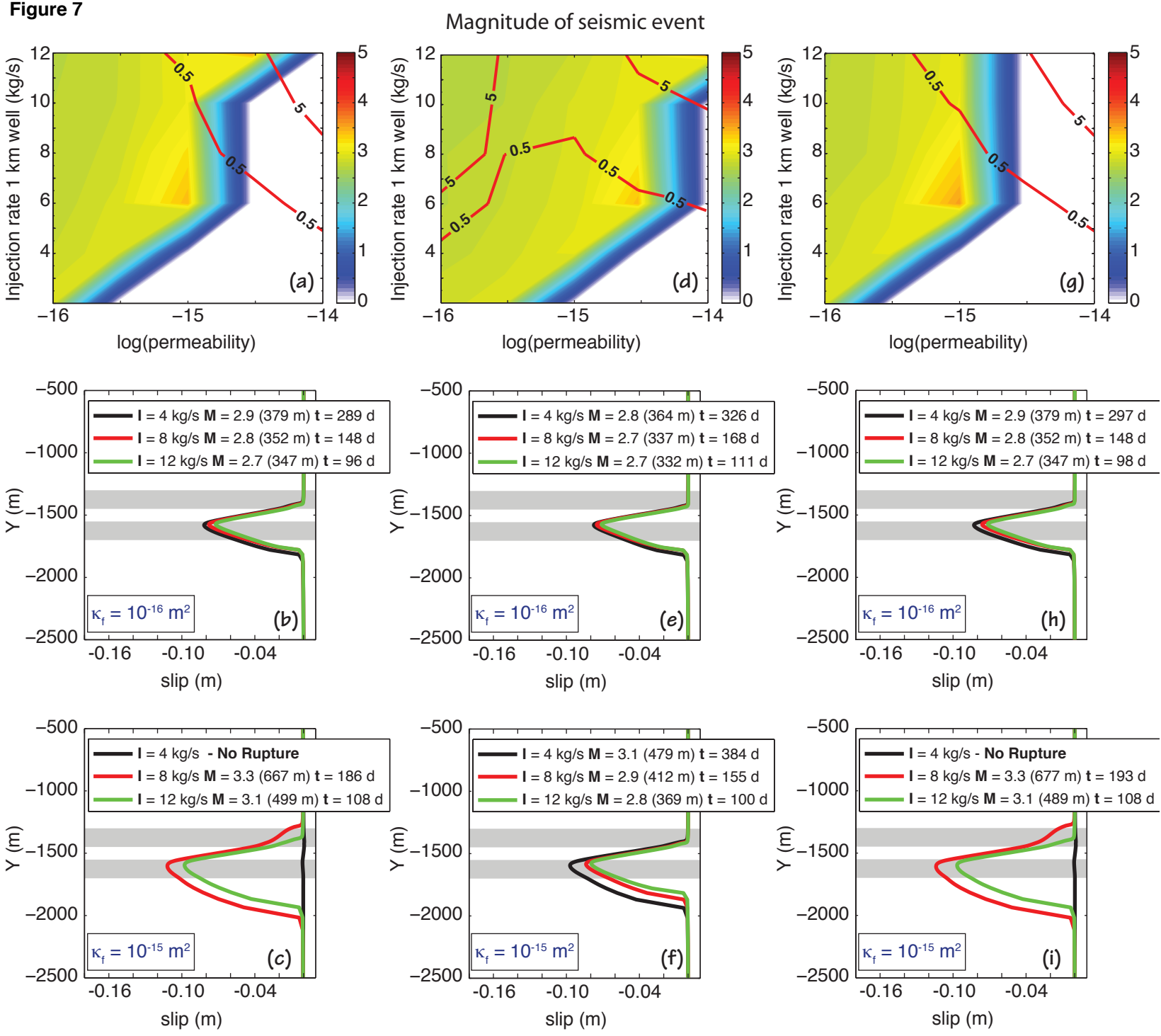
Magnitude of seismic event
Injection rate 1 km well (kg/s)
log(permeability)
(a)
(d)
(g)
I = 4 kg/s M = 2.9 (379 m) t = 289 d
I = 8 kg/s M = 2.8 (352 m) t = 148 d
I = 12 kg/s M = 2.7 (347 m) t = 96 d
I = 4 kg/s M = 2.8 (364 m) t = 326 d
I = 8 kg/s M = 2.7 (337 m) t = 168 d
I = 12 kg/s M = 2.7 (332 m) t = 111 d
I = 4 kg/s M = 2.9 (379 m) t = 297 d
I = 8 kg/s M = 2.8 (352 m) t = 148 d
I = 12 kg/s M = 2.7 (347 m) t = 98 d
κf = 10-16 m2
(b)
(e)
(h)
I = 4 kg/s - No Rupture
I = 8 kg/s M = 3.3 (667 m) t = 186 d
I = 12 kg/s M = 3.1 (499 m) t = 108 d
I = 4 kg/s M = 3.1 (479 m) t = 384 d
I = 8 kg/s M = 2.9 (412 m) t = 155 d
I = 12 kg/s M = 2.8 (369 m) t = 100 d
I = 4 kg/s - No Rupture
I = 8 kg/s M = 3.3 (677 m) t = 193 d
I = 12 kg/s M = 3.1 (489 m) t = 108 d
κf = 10-15 m2
(c)
(f)
(i)
Y (m)
slip (m)

Figure 8

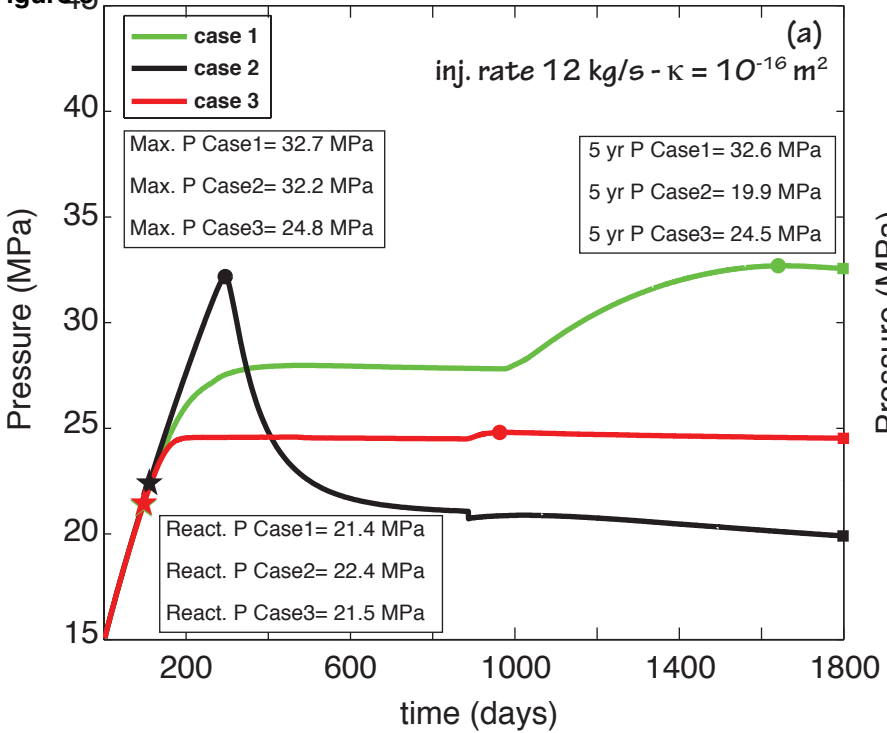
case 1
case 2
case 3
(a)
inj. rate 12 kg/s - κ = 10^-16 m^2
Max. P Case1= 32.7 MPa
Max. P Case2= 32.2 MPa
Max. P Case3= 24.8 MPa
5 yr P Case1= 32.6 MPa
5 yr P Case2= 19.9 MPa
5 yr P Case3= 24.5 MPa
React. P Case1= 21.4 MPa
React. P Case2= 22.4 MPa
React. P Case3= 21.5 MPa
Pressure (MPa)
time (days)
15
20
25
30
35
40
45
200
600
1000
1400
1800

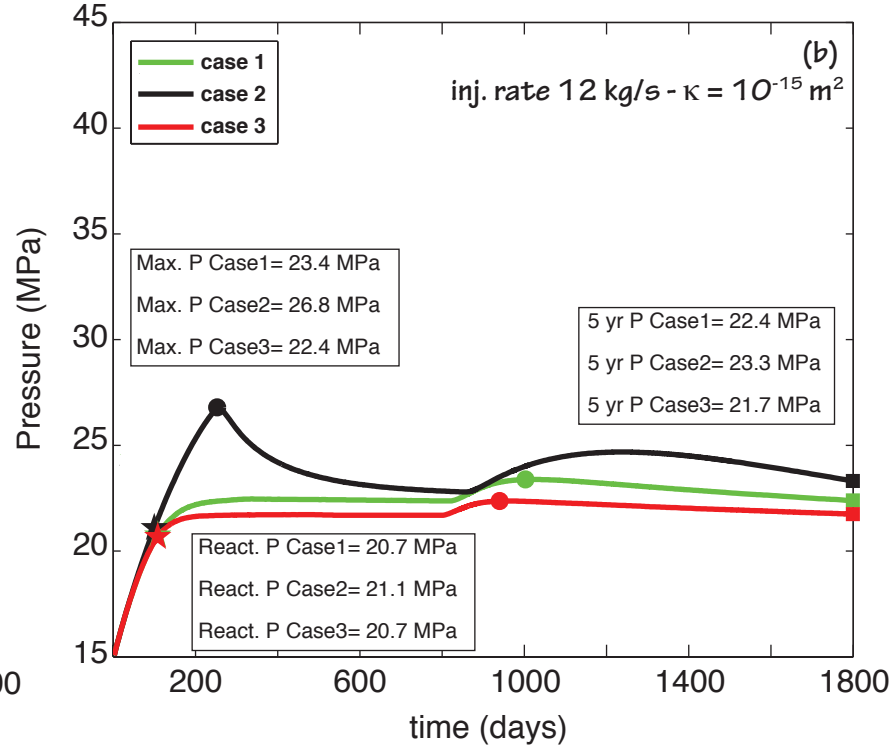
case 1
case 2
case 3
(b)
inj. rate 12 kg/s - κ = 10^-15 m^2
Max. P Case1= 23.4 MPa
Max. P Case2= 26.8 MPa
Max. P Case3= 22.4 MPa
5 yr P Case1= 22.4 MPa
5 yr P Case2= 23.3 MPa
5 yr P Case3= 21.7 MPa
React. P Case1= 20.7 MPa
React. P Case2= 21.1 MPa
React. P Case3= 20.7 MPa
Pressure (MPa)
time (days)
15
20
25
30
35
40
45
200
600
1000
1400
1800